Hippo/YAP Signaling Choreographs The Tumor Immune Microenvironment to Promote Triple Negative Breast Cancer Progression Via TAZ/IL-34 Axis

Zheng Wang (zhengwangwilson@163.com)
Department of General Surgery, Comprehensive Breast Health Center, Ruijin Hospital, Shanghai Jiao Tong University School of Medicine

Fan Wang
State Key Laboratory of Oncogenes and Related Genes, Renjin-MedX Stem Cell Research Center, Ren Ji Hospital, School of Medicine, Shanghai Jiao Tong University

Xin-Yuan Ding
Department of Pharmacy, the Affiliated Suzhou Hospital of Nanjing Medical University

Tian-En Li
Cancer Metastasis Institue, Fudan University

Hao-Yu Wang
Department of General Surgery, Comprehensive Breast Health Center, Ruijin Hospital, Shanghai Jiao Tong University School of Medicine

Yu-Hao Gao
The Brain Science Center, Beijing Institue of Basic Medical Sciences

Wen-Juan Wang
Department of Parmacy, Children's Hospital of Soochow University

Yan-Feng Liu
State Key Laboratory of Oncogenes and Related Genes, Renji-MedX Stem Cell Research Center, Ren Ji Hospital, School of Medicine, Shanghai Jiao Tong University

Xiao-Song Chen
Department of General Surgery, Comprehensive Breast Health Center, Ruijin Hospital, Shanghai Jiao Tong University School of Medicine

Kun-Wei Shen
Department of General Surgery, Comprehensive Breast Health Center, Ruijin Hospital, Shanghai Jiao Tong University School of Medicine

Research

Keywords: Triple-negative breast cancer, Hippo/YAP signaling, Anti-PD-L1, Tumor-associated macrophage, IL-34, Immunosuppressive microenvironment

Posted Date: May 21st, 2021

DOI: https://doi.org/10.21203/rs.3.rs-524972/v1

Version of Record: A version of this preprint was published at Cancer Letters on December 1st, 2021. See the published version at https://doi.org/10.1016/j.canlet.2021.12.016.

Abstract

Background: Growing evidence suggests that the bidirectional interactions between cancer cells and their surrounding environment namely the tumor microenvironment (TME), contributes to cancer progression, metastasis, and resistance to treatment. Intense investigation of Hippo pathway, which controls multiple central cellular function to tumorigenesis, was focused on cancer cells. However, the role of Hippo pathway in modulating tumor–stromal interactions in triple negative breast cancer remains largely unknow. This study therefore focused on revealing effects of Hippo-YAP/TAZ signaling to immune microenvironment.

Methods: The correlation between Hippo/YAP signaling and the abundance of immune cells were estimated by Immune Cell Abundance Identifier. Clinical TNBC samples from 120 patients were analyzed to assess the correlation between TAZ expression and disease prognosis as well as tumor-infiltrating immune cells. Inflammatory immune profiles, bioinformatics analysis and chromatin immunoprecipitation were performed to identify the expression of immune-related genes that were regulated by TAZ. An *in vitro* co-culture system was applied to investigate the crosstalk between TNBC cells and tumor-associated macrophages (TAMs) modulated by the TAZ/interleukin 34 (IL-34) axis. *In vivo* tumor growth and metastasis models were used to evaluate the pro-tumor functions of TAZ, IL-34, and TAMs as well as the antitumor efficacy of anti-PD-L1 and IL-34/colony-stimulating factor 1 receptor (CSF-1R) blockade.

Results: In TNBC patients, high activity of Hippo pathway was correlated with decreased number of T cells, upregulated TAM infiltration, and poor prognosis. TAZ could directly regulate IL-34 and PD-L1 expression and promote IL-34 secretion in TNBC cells, leading to increased TAM infiltration and distant metastasis. TAM-derived transforming growth factor beta 1 (TGF-β1) could also induce TAZ expression in TNBC cells, thus forming a positive feedback loop between TNBC cells and TAMs. Furthermore, targeting the TAZ/IL-34 axis through its CSF-1R inhibitor could dramatically decrease TAM infiltration and significantly improve anti-PD-L1 efficacy in inhibiting metastasis in TNBC.

Conclusions: Activity of Hippo pathway was associated with worse disease outcomes in TNBC and could increase TAM infiltration through the TAZ/IL-34 axis, leading to an immunosuppressive microenvironment and impairing the treatment efficacy of anti-PD-L1. Thus, the TAZ/IL-34 axis can serve as a novel target for TNBC patients.

Background

Triple-negative breast cancer (TNBC), accounting for 15–20% of all breast cancers [1], represents the most aggressive subtype and indicates a bad prognosis[2]. Due to the aggressive nature and lack of targeted therapies, numerous attempts have been made to develop viable targets for TNBC. Recent advances in immunotherapy have greatly improved cancer treatment by inhibiting immune checkpoints, such as programmed death 1 (PD-1) and its ligand programmed death ligand 1 (PD-L1)[3]. The

IMpassion130 trial showed the clinical success of the anti-PD-L1 drug atezolizumab in treating PD-L1-positive metastatic TNBC; the drug was approved as the first immune checkpoint inhibitor in breast cancer treatment[4]. However, the response rate of PD-1/PD-L1 antagonists has been unsatisfactory, mainly due to the immunosuppressive microenvironment of TNBC[5–7]. Therefore, it is important to reverse the immunosuppressive phenotype and enhance the antitumor efficacy of immune checkpoint blockade in TNBC patients.

Extensive studies have illustrated that interplay of cancer cells and the tumor microenvironment (TME) plays a significant role in ineffective treatment and poor prognosis of cancer. It's reported that cancer cells escape from immunosurveillance by producing immunosuppressive factors and recruiting suppressive immune cells—an important process known as the invasion-metastasis cascade [8]. Among suppressive immune cells, tumor-associated macrophages (TAMs) play a pivotal role in cancer metastasis and are predictive of poor prognosis in TNBC [9, 10]. Previous studies have also shown that immunosuppressive factors from cancer cells, such as C-C motif chemokine ligand 2, colony-stimulating factor 1 (CSF-1) and interleukin 4 (IL-4), promote TAM polarization and activation, thus forming an immunosuppressive microenvironment for cancer metastasis[11]. However, the mechanisms of TNBC-mediated TAM activation are not well understood.

The Hippo pathway, an evolutionarily conserved signaling, controls multiple significant cellular function and its dysregulation contributes to tumorigenesis. The Hippo pathway can promote tumor growth, stemness, and chemoresistance in human cancers including breast cancer[12]. Our group also found that yes-associated protein (YAP) modulated the crosstalk between breast cancer cells and their microenvironment[13]. However, the function and mechanism of the Hippo pathway in regulating the TNBC microenvironment remains unclear.

This study therefore aimed to explore the role of the Hippo pathway in the TNBC microenvironment and its influence on the antitumor effects of anti-PD-L1. Here, we identified the Hippo pathway remodeled the tumor immune microenvironment through mediating the proliferation and migration of TAMs and inhibiting T cell infiltration. Mechanistically, TAZ, the key regulators of Hippo signaling, facilitated TAM recruitment by directly modulating interleukin 34 (IL-34) transcription and decreased T cell infiltration by regulating PD-L1 expression in TNBC. Furthermore, we also identified an important positive feedback loop between TAZ and TAMs in the TNBC microenvironment. Thus, targeting TAMs through the IL-34/colony-stimulating factor 1 receptor (CSF-1R) inhibitor could enhance the antitumor efficacy of immune checkpoint blockade, making it a promising immunotherapy strategy for TNBC.

Methods

Patients and follow-up

Human breast cancer samples were collected from consecutive patients with TNBC who underwent surgery from 2009 to 2012 at the Comprehensive Breast Health Center, Ruijin Hospital, Shanghai Jiao

Tong University School of Medicine (Shanghai, China). All patients were histologically diagnosed by expert pathologists. A total of 120 patients diagnosed with TNBC were included in the study (Ruijin cohort), with a median follow-up of 84.6 months (range: 44.3-121.3 months). Overall survival (OS) was defined as the interval between the surgery date and the date of death or the last follow-up. Disease-free survival (DFS) was defined as the interval between the surgery date and the date of a reported event such as death, locoregional recurrence, contralateral breast cancer, distant metastasis, or second malignancy, or the date of the last follow-up. Patients' clinical characteristics are shown in Tables 1 and 2.

Table 1
Baseline clinical characteristics of TNBC patients.

Characteristics	Number (%)
Age at diagnosis, years	
≤ 50	45 (37.5%)
> 50	75 (62.5%)
Menopausal status	
Pre/Peri-menopausal	48 (40.0%)
Post-menopausal	72 (60.0%)
Location	
Left	64 (53.3%)
Right	56 (46.7%)
Tumor size, cm	
≤ 2	56 (46.7%)
> 2	64 (53.3%)
Regional Lymph node	
Negative	83 (69.2%)
Positive	37 (30.8%)
Histologic type	
IDC	103 (85.8%)
Non-IDC	17 (14.2%)
Histological grade	
I-II	30 (25.0%)
III	71 (59.2%)
Unknown	19 (15.8%)
Ki67, %	
≤ 14	17 (14.2%)
> 14	101 (84.2%)
Unknown	2 (16.7%)

BCS: breast-conserving surgery; IDC: invasive ductal carcinoma; TNBC: triple-negative breast cancer.

Characteristics	Number (%)
Breast surgery	
BCS	32 (26.7%)
Mastectomy	88 (73.3%)
Neoadjuvant chemotherapy	
No	106 (88.3%)
Yes	14 (11.7%)
Adjuvant chemotherapy	
No	6 (5.0%)
Yes	114 (95.0%)
Radiotherapy	
No	60 (50.0%)
Yes	60 (50.0%)
BCS: breast-conserving surgery; IDC: invasive ductal carcinoma; TNBC: triple-negative breast cancer.	

Table 2
Clinicopathological variables correlated with TAZ expression in TNBC patients.

Variable	TAZ low expression (n = 53)	TAZ high expression (n = 67)	*P*
Age at diagnosis, years			0.184
≤ 50	16 (30.2%)	29 (43.3%)	
> 50	37 (69.8%)	38 (56.7%)	
Menopausal status			0.456
Pre/Peri-menopausal	19 (35.8%)	29 (43.3%)	
Post-menopausal	34 (64.2%)	38 (56.7%)	
Location			0.583
Left	30 (56.6%)	34 (50.7%)	
Right	23 (43.4%)	33 (49.3%)	
Tumor size, cm			0.855
≤ 2	24 (45.3%)	32 (47.8%)	
> 2	29 (54.7%)	35 (52.2%)	
Regional Lymph node			0.427
Negative	39 (73.6%)	44 (65.7%)	
Positive	14 (26.4%)	23 (34.3%)	
Histologic type			0.444
IDC	44 (83.0%)	59 (88.1%)	
Non-IDC	9 (17.0%)	8 (11.9%)	
Histological grade			**0.022**
I-II	18 (33.9%)	12 (17.9%)	
III	24 (45.3%)	47 (70.2%)	
Unknown	11 (20.8%)	8 (11.9%)	
Ki67, %			**0.031**
≤ 14	12 (22.6%)	5 (7.4%)	

BCS: breast-conserving surgery; IDC: invasive ductal carcinoma; TAZ: transcriptional coactivator with PDZ-binding motif; TNBC: triple-negative breast cancer.

Variable	TAZ low expression (n = 53)	TAZ high expression (n = 67)	*P*
>14	41 (77.4%)	60 (89.6%)	
Unknown	0 (0%)	2 (3.0%)	
Breast surgery			0.099
BCS	10 (18.9%)	22 (32.8%)	
Mastectomy	43 (81.1%)	45 (67.2%)	
Neoadjuvant chemotherapy			0.152
No	44 (83.0%)	62 (92.5%)	
Yes	9 (17.0%)	5 (7.5%)	
Adjuvant chemotherapy			0.404
No	4 (7.5%)	2 (3.0%)	
Yes	49 (92.5%)	65 (97.0%)	
Radiotherapy			0.066
No	32 (60.4%)	28 (41.8%)	
Yes	21 (39.6%)	39 (58.2%)	

BCS: breast-conserving surgery; IDC: invasive ductal carcinoma; TAZ: transcriptional coactivator with PDZ-binding motif; TNBC: triple-negative breast cancer.

The present study was performed in accordance with the Declaration of Helsinki. Approval for the use of human subjects was obtained from the research ethics committee of Ruijin Hospital, Shanghai Jiao Tong University School of Medicine, and informed consent was obtained from each patient.

Immunohistochemistry

Immunohistochemistry (IHC) staining was applied using the avidin-biotin-peroxidase complex method, as previously described[14]. Briefly, after deparaffinization, rehydration, and antigen retrieval, the slides were incubated with the primary antibodies overnight at 4°C. The slides were then incubated with horseradish peroxidase-conjugated secondary antibodies (Abcam, UK) for 1 h at 37°C. After rinsing with phosphate buffer saline (PBS), the slides were stained with 3,3'-diaminobenzidine and counterstained with hematoxylin. The primary antibodies used are listed in Table 3.

Table 3

Primary antibodies for western blot, immunohistochemistry, immunofluorescence, and flow cytometry.

Protein	Concentration for WB	Concentration for IHC	Concentration for IF	Concentration for flow cytometry	Specificity	Company
TAZ	1:1000	1:200	/	/	Rabbit	CST
IL-34	1:1000	1:50	/	/	Mouse	Abcam
PD-L1	1:1000	1:30	/	/	Rabbit	Abcam
PD-L1	/	/	/	1:100	Rabbit	CST
p38	1:1000	/	/	/	Rabbit	CST
p-p38	1:1000	/	/	/	Rabbit	CST
mTOR	1:1000	/	/	/	Rabbit	CST
p-mTOR	1:1000	/	/	/	Rabbit	CST
F4/80	/	1:2400	/	/	Rabbit	CST
F4/80	/	/	/	1:100	Rat	BD Biosciences
CD206	/	1:2000	/	/	Rabbit	Abcam
CD206	/	/	/	1:100	Rat	BD Biosciences
CD68	/	1:2400	/	/	Rabbit	CST
CD4	/	1:1000	/	/	Rabbit	Abcam
CD4	/	/	/	1:100	Rat	BD Biosciences
CD8	/	1:800	1:200	/	Mouse	Thermo Scientific
CD8	/	/	/	1:100	Rat	BD Biosciences
CD45	/	/	/	1:100	Rat	BD Biosciences
CD11b	/	/	/	1:100	Rat	BD Biosciences
Ly6G	/	1:900	/	/	Rat	BioLegend

CST: Cell Signaling Technology; Foxp3: forkhead box protein P3; IF: immunofluorescence; IHC: immunohistochemistry; IL-34: interleukin 34; Ly6G: lymphocyte antigen 6 complex locus G6D; MPO: myeloperoxidase; PD-1: programmed death 1; PD-L1: programmed death ligand 1; TAZ: transcriptional coactivator with PDZ-binding motif; WB: western blot.

Protein	Concentration for WB	Concentration for IHC	Concentration for IF	Concentration for flow cytometry	Specificity	Company
MPO	/	1:600	/	/	Rabbit	Abcam
Foxp3	/	1:6000	/	/	Mouse	Abcam
Ki-67	/	1:100	/	/	Rabbit	Abcam
Caspase-3	/	1:600	/	/	Rabbit	CST
CD31	/	1:600	/	/	Rabbit	CST
α-tubulin	1:1000	/	/	/	Rabbit	Abclonal

CST: Cell Signaling Technology; Foxp3: forkhead box protein P3; IF: immunofluorescence; IHC: immunohistochemistry; IL-34: interleukin 34; Ly6G: lymphocyte antigen 6 complex locus G6D; MPO: myeloperoxidase; PD-1: programmed death 1; PD-L1: programmed death ligand 1; TAZ: transcriptional coactivator with PDZ-binding motif; WB: western blot.

IHC staining was independently and blindly evaluated by two researchers (including one expert pathologist). Under 200× magnification, photographs of three representative fields were captured under a microscope (Leica, Germany). For TAZ, IL-34, and PD-L1 staining in the tissue microarray detection, the scores were calculated as the percentage score multiplied by the staining intensity score. The percentage score of positive staining cells was defined as follows: 0, < 1%; 1, 1–25%; 2, 26–50%; 3, 51–75%; and 4, > 75%. Meanwhile, the staining intensity score was determined as follows: 0, negative; 1, weak positive; 2, moderate positive; and 3, strong positive. For CD8 and CD68 staining, the number of positive cells was calculated in a 0.5 mm diameter cylinder and expressed as the mean value of the triplicates (cells per spot). Median scores or values were used for correlation and survival analyses. Quantifications of F4/80, CD206, CD8, Ly6G, MPO, Foxp3, Ki-67, caspase-3, and CD31 staining in xenograft tumors were calculated as positive cells per field at 200× magnification in five areas of each slide.

Cell lines and animals

Mouse breast cancer cell lines 4T1 (ATCC, USA) and E0771 (CH3 BioSystems, USA) and human TNBC lines SUM1315 (Asterand, UK) and BT549 (ATCC) were used in this research. Human cell line HEK 293T and mouse macrophage cell line RAW264.7 (ATCC) were also used, as previously described[15]. These cell lines were routinely maintained in our laboratory.

Female BALB/c and C57BL/6 mice (5–6 weeks old; Shanghai SLAC Laboratory Animal Company, China) were used and housed under pathogen-free conditions. All animal experiments were approved by the Animal Ethics Committee of Ruijin Hospital and performed according to the “Guide for the Care and Use of Laboratory Animals” by the National Academy of Sciences (Washington, DC, USA).

Vectors and transfection

For stable expression of short hairpin RNAs (shRNAs), pLKO.1-shTAZ and pLKO.1-shIL-34 lentiviral vectors (Addgene, USA) were transfected into 4T1, E0771, SUM1315, and BT549 cells. A pCDH-IL-34 lentiviral vector (Addgene) was also transfected into TAZ-silenced 4T1 and E0771 cells to restore IL-34 expression. Moreover, an HA-TAZ-S89A lentiviral vector (Addgene) was used for overexpressing TAZ, as previously described[16]. Stably transfected clones were validated by real-time quantitative polymerase chain reaction (RT-qPCR) and western blot (WB). The targeting sequences of shRNAs, IL-34 overexpression, and TAZ S89A are listed in Table 4.

Table 4
shRNA, IL-34 overexpression and TAZ S89A primer sequences.

Gene		Sequences (5' → 3')
sh-TAZ 1#		CAGCCGAATCTCGCAATGAAT
sh-TAZ 2#		CCTGCATTTCTGTGGCAGATA
sh-TAZ 3#		GTGATGAATCAGCCTCTGAAT
sh-IL-34 1#		ACCGGCTTCAGTACATGAAAC
sh-IL-34 2#		CTCACGTGGAAGCTGTGTTAT
sh-IL-34 3#		AGCCCATGGGCCAGATCATTT
IL-34	Forward	ATGCCCTGGGGACTCGCCTGG
	Reverse	TCAGGGCAACGAGCCATGGCTT
TAZ S89A	Forward	ATGCCCCTCCATGTGAAGTG
	Reverse	CTATCTTCCAGGCTGGAAATGA

IL-34: interleukin 34; shRNA: short hairpin RNA; TAZ: transcriptional coactivator with PDZ-binding motif.

Protein extraction and WB

The cells and tissues were lysed with radioimmunoprecipitation assay buffer (RIPA) (Beyotime, China), and the protein level in the lysates was quantified using an enhanced bicinchoninic acid assay (BCA) kit (Thermo Scientific, USA). WB was performed as described previously[17]. The primary antibodies used are listed in Table 3.

RT-qPCR and RT^2 profiler PCR array

Xenograft tumors and cultured cells were lysed with TRIzolTM reagent (Invitrogen, USA), and RNA was isolated according to the manufacturer's instructions. RT-qPCR was performed using SYBR Green Realtime PCR Master Mix (Takara, Japan) in the ABI PRISM 7900 Sequence Detection System (Applied Biosystems, USA). Primer sequences for RT-qPCR analysis are shown in Table 5.

Table 5
Primers for RT-qPCR used in this study.

Gene	Sequences (5' → 3')	
mTAZ	Forward	CATGGCGGAAAAAGATCCTCC
	Reverse	GTCGGTCACGTCATAGGACTG
mIL-34	Forward	TTGCTGTAAACAAAGCCCCAT
	Reverse	CCGAGACAAAGGGTACACATTT
mPD-1	Forward	ACCCTGGTCATTCACTTGGG
	Reverse	CATTTGCTCCCTCTGACACTG
mPD-L1	Forward	GCTCCAAAGGACTTGTACGTG
	Reverse	TGATCTGAAGGGCAGCATTTC
mPD-L2	Forward	CTGCCGATACTGAACCTGAGC
	Reverse	GCGGTCAAAATCGCACTCC
mCTLA-4	Forward	GCTTCCTAGATTACCCCTTCTGC
	Reverse	CGGGCATGGTTCTGGATCA
mTIM-3	Forward	TCAGGTCTTACCCTCAACTGTG
	Reverse	GGGCAGATAGGCATTTTTACCA
mLAG-3	Forward	CTGGGACTGCTTTGGGAAG
	Reverse	GGTTGATGTTGCCAGATAACCC
mIL-1B	Forward	GCAACTGTTCCTGAACTCAACT
	Reverse	ATCTTTTGGGGTCCGTCAACT
mIL-12B	Forward	TGGTTTGCCATCGTTTTGCTG
	Reverse	ACAGGTGAGGTTCACTGTTTCT
miNOS	Forward	GTTCTCAGCCCAACAATACAAGA
	Reverse	GTGGACGGGTCGATGTCAC
mArg1	Forward	CTCCAAGCCAAAGTCCTTAGAG

Arg1: arginase 1; CTLA-4: cytotoxic T-lymphocyte associated protein 4; IL-1B: interleukin 1B; IL-10: interleukin 10; IL-12B: interleukin 12B; IL-34: interleukin 34; iNOS: inducible nitric oxide synthase; LAG-3: lymphocytes activation gene 3; PD-1: programmed death 1; PD-L1: programmed death ligand 1; PD-L2: programmed death ligand 2; TAZ: transcriptional coactivator with PDZ-binding motif; TGF-β1: transforming growth factor beta 1; TIM-3: T-cell immunoglobulin and mucin domain-containing protein 3.

Gene	Sequences (5' → 3')	
	Reverse	AGGAGCTGTCATTAGGGACATC
mIL-10	Forward	GCTCTTACTGACTGGCATGAG
	Reverse	CGCAGCTCTAGGAGCATGTG
mCD206	Forward	CTCTGTTCAGCTATTGGACGC
	Reverse	CGGAATTTCTGGGATTCAGCTTC
mTGF-β1	Forward	CTCCCGTGGCTTCTAGTGC
	Reverse	GCCTTAGTTTGGACAGGATCTG
hTAZ	Forward	GATCCTGCCGGAGTCTTTCTT
	Reverse	CACGTCGTAGGACTGCTGG
hIL-34	Forward	CCTGGCTGCGCTATCTTGG
	Reverse	AGTGTTTCATGTACTGAAGTCGG
hPD-L1	Forward	TGGCATTTGCTGAACGCATTT
	Reverse	TGCAGCCAGGTCTAATTGTTTT

Arg1: arginase 1; CTLA-4: cytotoxic T-lymphocyte associated protein 4; IL-1B: interleukin 1B; IL-10: interleukin 10; IL-12B: interleukin 12B; IL-34: interleukin 34; iNOS: inducible nitric oxide synthase; LAG-3: lymphocytes activation gene 3; PD-1: programmed death 1; PD-L1: programmed death ligand 1; PD-L2: programmed death ligand 2; TAZ: transcriptional coactivator with PDZ-binding motif; TGF-β1: transforming growth factor beta 1; TIM-3: T-cell immunoglobulin and mucin domain-containing protein 3.

Immune genes in xenograft tumors or TNBC cells with stable TAZ silencing and their control transfectants were screened using the RT^2 Profiler PCR Array System (RayBiotech, USA) and SYBR Green Realtime PCR Master Mix (Takara) in the ABI PRISM 7900 Sequence Detection System (Applied Biosystems), according to the manufacturer's instructions.

Macrophage proliferation assay

Macrophage proliferation was analyzed using Cell Counting Kit-8 (Dojindo, Japan). Cultured cells (RAW264.7) were dispensed into a 96-well plate at a density of 1000 cells/well, with or without a different level of IL-34 protein (Sino Biological, China) or conditioned medium (CM) from TNBC cells. To assess the IL-34-induced p38 and mTOR signaling pathways, the cells were treated with the CSF-1R inhibitor pexidartinib (AbMole, USA), the p38 inhibitor SB203580 (MedChemExpress, USA), or the mTOR inhibitor AZD8055 (MedChemExpress). At the indicated time points, the absorbance at 450 nm was measured to determine the number of viable cells in each well.

Macrophage chemotactic migration assay

Macrophage chemotactic migration assay was performed using a 24-well Transwell system, with upper and lower culture chambers separated by 8μm pore polycarbonate membranes (Corning, USA), as previously described[18]. The bottom chamber was filled with IL-34 protein in Dulbecco's modified eagle's medium (DMEM) (Hyclone, USA) containing 10% fetal bovine serum (Gibco, USA) or CM from TNBC cells. In the upper chambers, macrophages (RAW264.7, 5×10^4 cells/well) suspended in DMEM were seeded and then incubated for 24 h. Macrophages that migrated to the lower surface of the membrane were fixed in 4% paraformaldehyde, stained with Giemsa, and then photographed and counted with a light microscope (Leica). To assess the IL-34-induced p38 and mTOR signaling pathways, the cells were treated with selective inhibitors. The chemotactic index was calculated as the number of macrophages that migrated to IL-34 of the CM from TNBC cells divided by the number of macrophages that migrated to DMEM alone[19].

Macrophage isolation

For TAM isolation, xenograft tumors were collected and digested into single-cell suspensions as previously described[20], and macrophages were isolated using Anti-F4/80 MicroBeads (Miltenyi Biotec, Germany) according to the manufacturer's instructions.

Co-culture assay

A 6-well Transwell system with 0.4μm pore polycarbonate membranes (Corning) was used for the co-culture assay. TAMs (1×10^5 cells/well) isolated from xenograft tumors were seeded in the upper chambers and co-cultured with 4T1 or E0771 cells (1×10^5 cells/well) in the lower chambers for 48 h. The 4T1 or E0771 cells were re-plated and cultured, and after 12 h, supernatants were collected for further analysis.

Flow cytometry analysis

Xenograft tumors were dissected into small pieces and further digested into single cell suspensions. Cells were stained with antibodies and analyzed by flow cytometry (Epics Altra, USA) according to the manufacturer's instructions. The antibodies used are listed in Table 3.

Enzyme-linked immunosorbent assay and cytokine array analysis

IL-34 levels in cell culture supernatants were assessed using the mouse or human IL-34 enzyme-linked immunosorbent assay (ELISA) kit (RayBiotech) according to the manufacturer's instructions. Briefly, a sample solution was added to each well and incubated with an IL-34 conjugate. A substrate solution was then added, and the absorbance was analyzed using a microplate spectrophotometer (Bio-Rad, USA). A curve of the absorbance according to the IL-34 level in the standard wells was formulated.

The sample solution was collected from the cell culture supernatants of TAMs and then incubated with a biotinylated detection antibody cocktail and Cy3 equivalent dye-conjugated streptavidin from a mouse

cytokine array (RayBiotech). The signals were visualized with a microarray laser scanning system (GenePix, USA).

Phospho-kinase array analysis

The IL-34-induced downstream signaling pathways were analyzed using the mouse phosphorylation pathway array (RayBiotech). The protein lysate was incubated with the array membrane, and signaling proteins were visualized using a chemical fluorescence detection system (Bio-Rad) according to the manufacturer's instructions.

In vivo **tumor growth and metastasis assay**

For the xenograft tumor growth model, 4T1 or E0771 cells were orthotopically implanted into the mammary fat pad of BALB/c or C57BL/6 mice (1×10^5 cells/mouse). Tumor growth was monitored every 3 days, and tumor volume was calculated using the following formula: volume = $(\text{width})^2 \times \text{length} \div 2$. Tumor growth was visualized with a bioluminescence-based IVIS imaging system (Caliper Life Sciences, USA). Mice were sacrificed after 4 weeks, and tumor weight was then assessed and fixed in 4% paraformaldehyde solution for hematoxylin-eosin (H&E) and IHC staining.

For the metastatic model, 4T1 or E0771 cells were injected into the tail veins of BALB/c or C57BL/6 mice (5×10^4 cells/mouse). Four weeks later, the mice were sacrificed and the lungs were fixed in 4% paraformaldehyde solution for H&E staining. The number and the largest size of lung metastatic nodules were evaluated under a microscope (Leica).

For drug treatment, mice were randomly divided into four groups: immunoglobulin G (IgG) (Bio X Cell, USA) group (control), pexidartinib group, anti-PD-L1 group, and pexidartinib plus anti-PD-L1 group. Pexidartinib (40 mg/kg, AbMole) was given orally for 5 days every week, and anti-PD-L1 antibody (200μg/mouse, Bio X Cell) was injected intraperitoneally every 3 days.

Immunofluorescence

Briefly, slides were fixed in 4% paraformaldehyde for 15 min and then blocked with PBS containing 1% bovine serum albumin and 0.15% glycine for 1 h at room temperature. The slides were incubated with primary antibodies overnight at 4°C, and then incubated with Alexa Fluor secondary antibodies (Thermo Scientific) for 2 h. After rinsing with PBS, the slides were counterstained with 4',6-diamidino-2-phenylindole and evaluated by fluorescence microscopy (Leica).

Luciferase reporter assay

Cells with a stable knockdown of TAZ or S89A mutant TAZ and their control transfectants were plated into 24-well plates and transfected with pGL3-luciferase reporter plasmid and SV40 *Renilla* luciferase plasmid (Promega, USA). Cells were lysed and the luciferase activity was detected with a dual luciferase assay (Promega) according to the manufacturer's instructions.

Chromatin immunoprecipitation

Cells were crosslinked with 1% formaldehyde and incubated for 10 min at room temperature. Glycine was added into the medium for 10 min at room temperature to stop the crosslinking. After that, the cells were washed, lysed, resuspended, and sonicated to an average length of 500 base pairs. After centrifugation, the samples were incubated with primary antibodies (anti-TAZ, #4883, Cell Signaling Technology, UK; IgG-coated Dynabeads Protein A, #10001D, Invitrogen) overnight at 4°C, and then incubated with protein A/G beads at 4°C for 2 h. Magnetic beads were washed with lysis buffer twice, high salt buffer twice, LiCl buffer once, and TE buffer once successively on ice, and eluted with elution buffer. The eluents were reverse-crosslinked by adding 2 μL of 10 mg/mL RNase A at 37 for 1 h and 2 μL of 20 mg/mL protease K at 50°C for 1 h. De-crosslinked DNA was purified with a DNA purification kit (Qiagen, Germany) and eluted in nucleic acid-free water. RT-qPCR analysis was used to measure the enrichment of specific promoter regions. The RT-qPCR primers used for chromatin immunoprecipitation (ChIP) are shown in Table 6.

Table 6
Primer sequences for IL-34 and PD-L1 promoter used for ChIP.

ChIP primers		Sequences (5' → 3')
Primers for IL-34 promoter ChIP		
Primer 1 (-1053 ~ -804)	Forward	GCTTTTGTGGAGGGCCTTTG
	Reverse	GTAAAGGGCCACTCAAGGGA
Primer 2 (-509 ~ -352)	Forward	GCACAGGGCCTTGTCACTAT
	Reverse	CGCAGGGAGGTAGTTTACCC
Primers for PD-L1 promoter ChIP		
Primer 1 (-660 ~ -414)	Forward	ATGGCCCATTTCTGAGACCC
	Reverse	TTTTGGGTGGGAGTGGAACC
Primer 2 (-1324 ~ -1142)	Forward	CAGCGGACACCCCAGTATTC
	Reverse	TGCGAACTGGAAGTGTGGAC

ChIP: chromatin immuno-precipitation assay; IL-34: interleukin 34; PD-L1: programmed death ligand 1.

Bioinformatics and statistical analysis

RNA-seq data for TNBC patients and corresponding clinical information were downloaded from The Cancer Genome Atlas (TCGA) dataset. Meanwhile, the immune scores and the abundance of immune cells were estimated by Immune Cell Abundance Identifier (ImmuCellAI)[21]. According to the immune infiltration score, TNBC samples were divided into high- and low- infiltration group to analyze the activity of conserved YAP signature by GSVA algorithm[22].The cBioPortal for Cancer Genomics, a web-based tool for analyzing RNA-Seq data from The Cancer Genome Atlas (TCGA), was used to evaluate the correlation between the mRNA expression of TAZ and cytokines/chemokines in the TCGA cohort[23]. The

Kaplan-Meier Plotter, a web-based application, was used to assess the impact of TAZ expression on the prognosis of TNBC patients[24].

Statistical analysis was performed using GraphPad Prism 7 (GraphPad, USA) and SPSS 22.0 (SPSS Inc., USA). Quantitative data were presented as means and standard errors of the mean, and qualitative values were shown as numbers. Unpaired Student's *t* test, one-way analysis of variance (ANOVA), or two-way ANOVA was performed for quantitative data as appropriate. The chi-squared test or Fisher's exact test was applied to analyze the correlation between qualitative variables, and Pearson's correlation test to analyze the correlation between quantitative variables. Kaplan-Meier curves were used to assess the impact of prognostic factors on patient survival. Two-sided $P < 0.05$ was considered statistically significant and was marked as * $P < 0.05$, ** $P < 0.01$, *** $P < 0.001$.

Results

High Hippo pathway activity was positively correlated with the immunosuppressive microenvironment and poor prognosis in TNBC patients

The finding that nuclear translocation of YAP mediating resistance to anti-PD-1 immunotherapy[25] lead us to assess the relationship between YAP/TAZ signaling and immune phenotype in TNBC. We firstly discovered higher level of conserved YAP signature was significantly correlated with higher immune infiltration score (Fig. 1A) and worse patient outcome (Fig. 1B). Noteworthily, the infiltration of $CD8^+$ T-cell was more in the group with lower level of conserved YAP signature, while the infiltration of macrophage was quite contrary ((Fig. 1C), thus forming an immunosuppressive microenvironment. Then we detected the levels of TAZ, $CD8^+$ T cells, and $CD68^+$ TAMs in TNBC patient samples by IHC staining (Fig. 1D). Notably, TAZ expression was negatively associated with the number of $CD8^+$ T cells ($r = -0.577$, $P < 0.0001$) (Fig. 1E) but positively associated with the number of $CD68^+$ TAMs ($r = 0.606$, $P < 0.0001$) (Fig. 1F), indicating that YAP/TAZ signaling was positively correlated with the immunosuppressive microenvironment in TNBC patients.

Kaplan-Meier curves showed that both 5-year OS and DFS in TNBC patients with high TAZ expression were significantly lower than those of patients with low TAZ expression (OS: 85.1% vs 98.1%; DFS: 80.6% vs 96.2%) (Fig. 1G). Similarly, the Kaplan-Meier Plotter analysis also revealed that TNBC patients with high TAZ expression showed an unfavorable prognosis compared to those with low TAZ expression (Figure S1A-B). The 5-year OS and DFS in TNBC patients with an increased number of intratumoral $CD8^+$ T cells were 98.4% and 95.3%, respectively, which were significantly higher than those with fewer $CD8^+$ T cells (82.1% and 78.6%) (Fig. 1H). Meanwhile, TNBC patients with increased TAM infiltration displayed significantly poorer 5-year OS and DFS than those with decreased TAM infiltration (OS: 85.2% vs 96.6%; DFS: 80.3% vs 94.9%) (Fig. 1I). Furthermore, to assess the combined effects of TAZ, T cells and TAMs on prognosis, we stratified the TNBC patients into three groups (Group I: patients with low TAZ expression, an increased number of T cells, and fewer TAMs; Group III: patients with high TAZ expression, fewer T cells, and an increased number of TAMs; and Group II: the remaining patients). The 5-year OS in groups I,

II, and III were 100.0%, 94.7%, and 65.0%, respectively (Fig. 1J). Meanwhile, the 5-year DFS in group I was 100.0%, which was significantly higher than that of group II (89.3%) and group III (65.0%) (Fig. 1J). Therefore, the high expression of TAZ was positively correlated with fewer T cells while the increase in TAM infiltration was associated with poor prognosis in TNBC patients.

Hippo pathway promoted TNBC growth and metastasis by driving the immunosuppressive tumor microenvironment

To explore the role of Hippo pathway in the immunosuppressive microenvironment of TNBC, we stably silenced TAZ expression in mouse breast cancer cells and established a tumor orthotopic transplantation model with these cells. We found that the tumor sizes and weights in 4T1-shTAZ and E0771-shTAZ xenograft tumors were significantly lower than those of the control groups (Fig. 2A-B and S2A-B). The number and the largest diameter of metastatic nodules significantly decreased in the shTAZ mice than in the control group (Fig. 2C-D and S2C). Additionally, IHC staining and flow cytometry analysis showed an increased number of $CD8^+$ T cells and fewer $F4/80^+$ $CD206^+$ TAMs in the 4T1-shTAZ and E0771-shTAZ xenograft tumors (Fig. 2E-H and S3), whereas TAZ silencing did not reduce the number of other tumor-infiltrating immune cells (Figure S2D-E). Collectively, these results confirmed that Hippo pathway indeed decreased intratumoral T cell infiltration but promoted TAM recruitment, thus forming an immunosuppressive microenvironment, and promoting TNBC growth and metastasis.

TAZ directly regulated IL-34 and PD-L1 expression

To figured out how Hippo pathway modulated immune cell infiltration in TNBC, GSEA analysis of TNBC patient datasets revealed that high expression of TAZ enriched expression of cytokines and chemokines production (Fig. 3A). To identify cytokines or chemokines that may be regulated by TAZ, the RT^2 profiler PCR array was employed. The effect of TAZ on the expression of immune genes (including 57 cytokines/chemokines and 25 immune checkpoints) was presented as downregulation of cytokines/chemokines in 4T1-shTAZ- and E0771-shTAZ-derived xenograft tumors and SUM1315-shTAZ and BT549-shTAZ cells (Table 7–8 and Figure S4A). As shown in the Venn diagram (Fig. 3B), only IL-34 was shared by all of the above groups. Notably, TAZ expression was positively associated with the expression of IL34 in TCGA TNBC patients (Fig. 3C). RT-qPCR, WB, and IHC showed that TAZ silencing significantly decreased IL-34 expression in TNBC cells and xenograft tumors (Fig. 3D&E and S4B). ELISA testing also indicated that IL-34 secretion was reduced in TAZ-silenced TNBC cells (Fig. 3D). Furthermore, luciferase reporter and ChIP assays on 4T1 and E0771 cell lines were performed to determine if TAZ could regulate IL-34 transcription; indeed, TAZ activated IL-34 transcription by directly binding to specific regions on the IL-34 promoter (Fig. 3F and S4C-E).

Table 7
Changes in the expression levels of immune genes in xenograft tumors.

E0771-shTAZ vs shCtrl	Fold change (low to high)	4T1-shTAZ vs shCtrl	Fold change (low to high)
CD278	0.198	IL-34	0.270
CXCL13	0.345	PD-L1	0.279
PD-L1	0.354	CXCL5	0.288
IL-34	0.380	IL-9	0.339
CD28	0.388	IL-3	0.375
CCL11	0.390	Arg1	0.378
IL-10	0.396	IL-10	0.382
OX40L	0.412	CTLA-4	0.432
IL-7	0.436	CCL2	0.435
CCL26	0.438	CCL22	0.478
IL-2	0.449	CXCL1	0.492
CXCL10	0.487	CCL21	0.496
Ptgs2	0.489		
CD154	0.494		
IL-15	0.508		
IL-5	0.516		
Arg1	0.520		
IL-17A	0.524		
IL-22	0.548		
IDO	0.557		
IL-21	0.562		
Galectin9	0.565		
IL-18	0.575		

E0771- shTAZ vs shCtrl	Fold change (low to high)	4T1- shTAZ vs shCtrl	Fold change (low to high)

Arg1: arginase 1; CCL2: C-C motif chemokine ligand 2; CCL11: C-C motif chemokine ligand 11; CCL21: C-C motif chemokine ligand 21; CCL22: C-C motif chemokine ligand 22; CCL26: C-C motif chemokine ligand 26; CTLA-4: cytotoxic T-lymphocyte associated protein 4; CXCL1: C-X-C motif chemokine ligand 1; CXCL5: C-X-C motif chemokine ligand 5; CXCL10: C-X-C motif chemokine ligand 10; CXCL13: C-X-C motif chemokine ligand 13; IDO: indoleamine 2, 3-dioxygenase; IL-2: interleukin 2; IL-3: interleukin 3; IL-7: interleukin 7; IL-9: interleukin 9; IL-10: interleukin 10; IL-15: interleukin 15; IL-17A: interleukin 17A; IL-18: interleukin 18; IL-21: interleukin 21; IL-22: interleukin 22; IL-34: interleukin 34; PD-L1: programmed death ligand 1; Ptgs2: prostaglandin-endoperoxide synthase 2; TAZ: transcriptional coactivator with PDZ-binding motif; TNBC: triple-negative breast cancer.

Table 8
Changes in the expression levels of cytokines/chemokines in TNBC cells.

SUM1315-shTAZ vs shCtrl	Fold change (low to high)	BT549-shTAZ vs shCtrl	Fold change (low to high)
CXCL5	0.169	IL-10	0.111
IL-34	0.173	IFNG	0.166
CSF-1	0.178	IL-34	0.172
CCL2	0.186	CSF-3	0.188
IL-7	0.217	IL-4	0.212
CSF-3	0.311	IL-6	0.216
IL-12A	0.313	IL-7	0.227
CXCL6	0.339	CXCL1	0.269
CCL21	0.390	CXCL2	0.275
CCL5	0.445	IL-13	0.285
CXCL12	0.523	TNF	0.311
		CXCL10	0.324
		CCL20	0.372
		CCL4	0.379
		CXCL3	0.454
		CCL2	0.498
		CSF-1	0.516
		IL-16	0.528
		IL-12B	0.535
		CCL18	0.559

CCL2: C-C motif chemokine ligand 2; CCL4: C-C motif chemokine ligand 4; CCL5: C-C motif chemokine ligand 5; CCL18: C-C motif chemokine ligand 18; CCL20: C-C motif chemokine ligand 20; CCL21: C-C motif chemokine ligand 21; CSF-1: colony-stimulating factor 1; CSF-3: colony-stimulating factor 3; CXCL1: C-X-C motif chemokine ligand 1; CXCL2: C-X-C motif chemokine ligand 2; CXCL3: C-X-C motif chemokine ligand 3; CXCL5: C-X-C motif chemokine ligand 5; CXCL6: C-X-C motif chemokine ligand 6; CXCL10: C-X-C motif chemokine ligand 10; CXCL12: C-X-C motif chemokine ligand 12; IFNG: interferon gamma; IL-4: interleukin 4; IL-6: interleukin 6; IL-7: interleukin 7; IL-10: interleukin 10; IL-12A: interleukin 12A; IL-12B: interleukin 12B; IL-13: interleukin 13; IL-16: interleukin 16; IL-34: interleukin 34; TNF: tumor necrosis factor.

In the RT-qPCR-based assay, in addition to IL-34, we found that PD-L1 was also a gene targeted by TAZ. TAZ silencing significantly decreased PD-L1 expression in 4T1 and E0771 xenograft tumors (Fig. 3G and S5A), which was confirmed by the results of IHC (Fig. 3H and S5B). Furthermore, TAZ showed a high affinity to specific regions on the PD-L1 promoter in the luciferase reporter and ChIP assays (Fig. 3I and S5C-E). Clinically, TAZ expression was positively associated with IL-34 and PD-L1 expression, while IL-34 was positively correlated with $CD68^+$ TAMs in TNBC samples (Fig. 3J and S4F). Additionally, high expression of IL-34 or PD-L1 was associated with poor prognosis in TNBC patients (Fig. 3K and S4G, S5F&G). Thus, Hippo/YAP signaling could directly mediate PD-L1 and IL-34 expression in TNBC.

The TAZ/IL-34 axis promoted proliferation and migration of macrophages by activating the p38 and mTOR signaling pathways

Given that IL-34 is a newly discovered cytokine, which specifically binds to its receptor, CSF-1R, and regulates the development, differentiation, and function of monocytes and macrophages[26], we next examined the role of IL-34 in macrophage proliferation and chemotactic migration *in vitro*. Indeed, we found that IL-34 could lead to concentration-dependent proliferation and chemotactic migration of macrophages (Fig. 4A&B). The phospho-kinase array and WB indicated that IL-34 increased the phosphorylation levels of p38 and mTOR, which could be inhibited by the CSF-1R inhibitor pexidartinib, a p38 inhibitor, or an mTOR inhibitor (Fig. 4C&D). The enhanced macrophage proliferation and migration could also be abolished by these inhibitors, indicating that IL-34 could induce the activation of the p38 and mTOR signaling pathways in macrophages (Fig. 4E&F). In addition, the CM from 4T1 or E0771 cells could enhance the proliferative and migratory abilities of macrophages, which could be suppressed by TAZ or IL-34 silencing, whereas IL-34 overexpression rescued the TAZ silencing-induced inhibition of the proliferative and migratory effects of 4T1 or E0771 cells on macrophages (Fig. 4G-I). Therefore, YAP/TAZ signaling could promote proliferation and migration of macrophages by upregulating the IL-34-mediated activation of the p38 and mTOR signaling pathways.

The TAZ/IL-34 axis contributed to tumor progression by inducing TAM infiltration

Considering the role of YAP/TAZ signaling in TAM activation, we performed *in vivo* assays to study the effect of the TAZ/IL-34 axis on regulating TAM activation and TNBC progression. In 4T1 and E0771 cells, TAZ or IL-34 silencing mitigated the tumor growth and metastasis, while IL-34 overexpression rescued the TAZ silencing-induced inhibition of TNBC progression (Fig. 5A-D and S6A-D).

We performed IHC staining and flow cytometry to evaluate TAM infiltration in xenograft tumors, and the results indicated that TAZ or IL-34 silencing decreased the number of $F4/80^+$ $CD206^+$ TAMs, while IL-34 overexpression rescued the TAZ silencing-induced reduction of TAM infiltration (Fig. 5E-H). We also found that TAZ silencing downregulated the expression of macrophage M2 markers arginase 1 (Arg1), interleukin 10 (IL-10), and mannose receptor (CD206), which could be rescued by IL-34 overexpression (Figure S6E). Hence, the TAZ/IL-34 axis contributed to tumor progression by inducing TAM infiltration.

TAZ functioned as a feedback mechanism inducing TAM infiltration to promote TNBC progression

To further study the crosstalk between cancer cells and TAMs, we generated a co-culture model (Fig. 6A). As expected, we found that the CM from 4T1 or E0771 cells could promote the proliferative and migratory abilities of macrophages, which were abolished by TAZ or IL-34 silencing (Fig. 6B-C). Interestingly, after co-culture with TAMs, 4T1 and E0771 cells showed an upregulation in TAZ expression and IL-34 and PD-L1 expression (Fig. 6D). To clarify the mechanism of increased TAZ expression in 4T1 and E0771 cells by TAMs, a cytokine array was conducted and showed that the most predominantly secreted cytokines by TAMs were transforming growth factor beta 1 (TGF-β1), C-X-C motif chemokine ligand 12, C-C motif chemokine ligand 1 (CCL1), CCL5, and CCL3 (Fig. 6E). Furthermore, anti-TGF-β1 neutralizing antibody significantly abrogated the TAM-induced upregulation of TAZ expression, whereas other neutralizing antibodies had no impact on TAZ expression (Fig. 6F). Therefore, TAM-derived TGF-β1 could promote the expression of TAZ, thereby forming a positive feedback loop to induce IL-34-mediated TAM infiltration in TNBC.

CSF-1R blockade sensitized TNBC to anti-PD-L1-mediated immunotherapy by reversing the immunosuppressive tumor microenvironment

Regarding the ability of TAMs to suppress T cell antitumor immune response[27], we investigated whether targeting TAMs through its CSF-1R inhibitor and inhibiting T cell antitumor response by anti-PD-L1 blockade could synergistically inhibit tumor progression in TNBC. The mice with orthotopic 4T1 and E0771 cells were treated with an isotype control antibody, the CSF-1R inhibitor pexidartinib, and anti-PD-L1, or a combination of pexidartinib and anti-PD-L1 (Figure S7A&B). The results showed that the combination of pexidartinib and anti-PD-L1 significantly mitigated tumor growth (Fig. 7A-C and S8A-E) and inhibited lung metastasis (Fig. 7D-E and S8F-I), without any significant effect on mice body weight or toxicity in the liver and kidneys (Figure S7C-E). Thus, CSF-1R signaling blockade and anti-PD-L1 blockade could result in a synergistic antitumor response in TNBC.

To further clarify the mechanism underlying the synergistic antitumor effect of the pexidartinib and anti-PD-L1 combination, the number of tumor-infiltrating immune cells in xenograft tumors was analyzed by IHC staining and flow cytometry. As expected, we observed a significant reduction in TAMs in the pexidartinib plus anti-PD-L1 treatment group and an increased number of $CD8^+$ T cells in the combined treatment group (Fig. 7F, 7H, S9A and S9C). Immunofluorescence staining further validated the increase in the number of intratumoral $CD8^+$ T cells in the combined treatment group (Fig. 7G and S9B). Furthermore, Ki-67 and CD31 expression were significantly mitigated in the pexidartinib and anti-PD-L1 group, while caspase-3 expression was upregulated in the combined treatment group (Figure S10A-B). Hence, the combination of pexidartinib and anti-PD-L1 treatment inhibited the proliferation and angiogenesis of cancer cells and promoted their apoptosis, thus enhancing the antitumor effect in TNBC.

Consequently, a working model was proposed based on these results (Fig. 8). YAP/TAZ signaling drives the immunosuppressive phenotype in TNBC by decreasing intratumoral T cell infiltration and promoting TAM recruitment. As a signaling hub in the tumor microenvironment, YAP/TAZ signling shifts the immune and inflammatory profile and directly regulates IL-34 and PD-L1 expression. IL-34 promotes the proliferation and migration of TAMs by activating the p38 and mTOR signaling pathways. TAM-derived TGF-β1 promotes TAZ expression in TNBC cells, thus forming a positive feedback loop between TNBC cells and TAMs. Blocking the TAZ/IL-34/CSF-1R axis reduces TAM infiltration, activates intratumoral $CD8^+$ T cells, and sensitizes TNBC to anti-PD-L1-mediated immunotherapy.

Discussion

The immunosuppressive microenvironment of TNBC is critical for TNBC metastasis. Although previous studies have investigated the intrinsic impact of the Hippo pathway on cancer cell biology, the relationship between the Hippo pathway and the immunosuppressive tumor microenvironment remains not well understood. In this study, we found that the Hippo pathway remodeled the tumor immune microenvironment through mediating the proliferation and migration of TAMs by regulating the IL-34/CSF-1R axis, and inhibiting T cell infiltration by upregulating the expression of the immune checkpoint PD-L1, thus forming an immunosuppressive microenvironment in TNBC.

We firstly found that higher level of Hippo pathway was significantly correlated with decreased number of $CD8^+$ T cells, upregulated TAM infiltration, and poor prognosis in TNBC patients. Moreover, TNBC patients with an immunosuppressive phenotype showed an unfavorable prognosis and a high probability of tumor relapse. In supporting these findings, TAZ silencing in 4T1 and E0771 cells remarkably inhibited tumor cell growth and metastasis, mainly through downregulating TAM infiltration and increasing $CD8^+$ T cell infiltration. These findings indicate that Hippo pathway has a novel function in remodeling the tumor immune microenvironment. Whether TAZ is involved in the immunosuppressive microenvironment of other tumors requires further in-depth studies.

To explore the molecular mechanism of the Hippo pathway mediated immunosuppressive microenvironment in TNBC, we performed gene expression profiling and bioinformatics analysis and found that TAZ could shift the immune and inflammatory profile and directly regulate IL-34 expression in both TNBC cells and tissues. IL-34, a newly identified cytokine whose specific binding receptor is CSF-1R, is important in modulating macrophage proliferation, migration, and colonization[26]. Previous studies suggested that IL-34 regulated the immune response in chronic inflammatory disease [28, 29] and promoted disease progression and chemoresistance in lung and ovarian cancers[30, 31]. However, the role of IL-34 in TNBC remains unclear. In this study, we found that the TAZ/IL-34 axis mediated cancer progression by recruiting TAMs and predicted poor prognosis in TNBC patients. Moreover, IL-34 induced the activation of the p38 and mTOR signaling pathways in the macrophages. Thus, the TAZ/IL-34 axis has a critical role in promoting TNBC metastasis.

Various immune cells are recruited into the tumor bed depending on the inflammatory factors secreted by the cancer cells, and these immune cells are reported to exhibit pro-tumor phenotypes[32]. Among these tumor-infiltrating immune cells, TAMs are particularly abundant in TNBC[33]. Several studies have substantially proven that intratumoral TAMs facilitate cancer progression and metastasis by promoting cancer cell proliferation, migration, and angiogenesis[34, 35]. To further investigate the mechanism by which TAMs affect TNBC progression, we isolated macrophages from xenograft tumors; we found that TGF-β1 was the most predominant cytokine secreted by TAMs. TGF-β1 activates the polarization of several immune cells and mediates the immunosuppressive microenvironment[36]. TGF-β1 also upregulates TAZ expression via an SMAD3-dependent or SMAD3-independent mechanism[37, 38], but this phenomenon is not clearly understood in TNBC. In this study, we confirmed that TAM-derived TGF-β1 positively regulated TAZ expression in TNBC cells. Further in-depth studies are recommended to investigate whether SMAD3 affects the role of TGF-β1 in promoting TAZ expression. Collectively, our results demonstrate the presence of a TAZ/IL-34/TAM feedback loop in TNBC growth and metastasis.

The gene expression profiles in this study also revealed that the immune checkpoint PD-L1 was a gene targeted by TAZ. Consistent with the findings of a previous report[39], we found that TAZ promoted PD-L1 expression in both TNBC cells and tissues. Upregulation of PD-L1 and its ligation to PD-1 on T cells can trigger inhibitory signals, mitigate T cell antitumor response, and bypass immunosurveillance[40]; these mechanisms may explain the unfavorable survival outcome of patients in our study. Although anti-PD-L1 blockade has been clinically applied in the treatment of TNBC, its response rate and long-term benefits are limited due to the presence of pre-existing immunosuppressive factors, especially TAMs[41, 42]. So there comes the need of developing new strategies to reverse the pre-existing immunosuppressive microenvironment and enhance the efficacy of immune checkpoint inhibitors in TNBC immunotherapy. In this study, the CSF-1R inhibitor pexidartinib significantly inhibited tumor growth and metastasis in combination with anti-PD-L1 blockade in mouse models. Moreover, the combined therapy significantly decreased TAM infiltration and activated $CD8^+$ T cell response, thus reversing the immunosuppressive microenvironment in TNBC. CSF-1R inhibitors are considered novel targets in the treatment of solid tumors other than TNBC[43–45]. To our knowledge, this is the first study to explore the novel therapeutic benefits of using the CSF-1R inhibitor pexidartinib in combination with anti-PD-L1 blockade in the treatment of TNBC.

In conclusion, this study revealed that Hippo pathway was associated with worse disease outcomes in TNBC and could increase the infiltration of tumor-associated macrophages through the TAZ/IL-34 axis, specifically through its CSF-1R, leading to an immunosuppressive microenvironment and impairing the treatment efficacy of anti-PD-L1. Therefore, targeting the TAZ/IL-34 axis can be a novel immunotherapy strategy in the treatment of TNBC.

Conclusions

Altogether, we found that the Hippo pathway effector TAZ contribute to the bidirectional interactions between cancer cells and the TME in TNBC. We deciphered TAZ mediated the proliferation and migration

of TAMs by regulating the IL-34/CSF-1R axis, and inhibited T cell infiltration by upregulating the expression of the immune checkpoint PD-L1, thus forming an immunosuppressive microenvironment in TNBC. Our findings unveil the CSF-1R inhibitor pexidartinib in combination with anti-PD-L1 blockade can be used as a novel potential therapeutic approach for TNBC.

Abbreviations

ANOVA: analysis of variance; Arg1: arginase 1; BC: breast cancer; BCA: bicinchoninic acid assay; BCS: breast-conserving surgery; CCL1: C-C motif chemokine ligand 1; CCL2: C-C motif chemokine ligand 2; CCL3: C-C motif chemokine ligand 3; CCL4: C-C motif chemokine ligand 4; CCL5: C-C motif chemokine ligand 5; CCL11: C-C motif chemokine ligand 11; CCL18: C-C motif chemokine ligand 18; CCL20: C-C motif chemokine ligand 20; CCL21: C-C motif chemokine ligand 21; CCL22: C-C motif chemokine ligand 22; CCL26: C-C motif chemokine ligand 26; CD206: mannose receptor; ChIP: chromatin immuno-precipitation assay; CM: conditioned medium; CTLA-4: cytotoxic T-lymphocyte associated protein 4; CSF-1: colony-stimulating factor 1; CSF-3: colony-stimulating factor 3; CSF-1R: colony-stimulating factor 1 receptor; CXCL1: C-X-C motif chemokine ligand 1; CXCL2: C-X-C motif chemokine ligand 2; CXCL3: C-X-C motif chemokine ligand 3; CXCL5: C-X-C motif chemokine ligand 5; CXCL6: C-X-C motif chemokine ligand 6; CXCL10: C-X-C motif chemokine ligand 10; CXCL12: C-X-C motif chemokine ligand 12; CXCL13: C-X-C motif chemokine ligand 13; DAPI: diamidino phenylindole; DFS: disease-free survival; DMEM: Dulbecco's modified eagle's medium; ELISA: enzyme linked immunosorbent assay; Foxp3: forkhead box protein P3; H&E: hematoxylin-eosin; IDC: invasive ductal carcinoma; IDO: indoleamine 2, 3-dioxygenase; IF: immunofluorescence; IFNG: interferon gamma; IgG: immunoglobulin G; OS: overall survival; IHC: immunohistochemistry; IL-2: interleukin 2; IL-3: interleukin 3; IL-4: interleukin 4; IL-6: interleukin 6; IL-7: interleukin 7; IL-9: interleukin 9; IL-10: interleukin 10; IL-12A: interleukin 12A; IL-12B: interleukin 12B; IL-13: interleukin 13; IL-15: interleukin 15; IL-16: interleukin 16; IL-17A: interleukin 17A; IL-18: interleukin 18; IL-21: interleukin 21; IL-22: interleukin 22; IL-34: interleukin 34; LAG-3: lymphocytes activation gene 3; Ly6G: lymphocyte antigen 6 complex locus G6D; MPO: myeloperoxidase; PBS: phosphate buffer saline; PD-1: programmed death 1; PD-L1: programmed death ligand 1; PD-L2: programmed death ligand 2; Ptgs2: prostaglandin-endoperoxide synthase 2; RFS: recurrence-free survival; RIPA: radioimmunoprecipitation assay buffer; RT-qPCR: real-time quantitative polymerase chain reaction; shRNA: short hairpin RNA; TAM: tumor-associated macrophage; TAZ: transcriptional coactivator with PDZ-binding motif; TCGA: The Cancer Genome Atlas; TGF-β1: transforming growth factor beta 1; TIM-3: T-cell immunoglobulin and mucin domain-containing protein 3; TNBC: triple-negative breast cancer; TNF: tumor necrosis factor; WB: western blot; YAP: yes-associated protein.

Declarations

Ethics approval and consent to participate

The present study was performed in accordance with the Declaration of Helsinki. Approval for the use of human subjects was obtained from the research ethics committee of Ruijin Hospital, Shanghai Jiao Tong

University School of Medicine, and informed consent was obtained from each patient.

Consent for publication

Not applicable.

Availability of data and materials

The datasets used and/or analyzed during the current study are available from the corresponding author on reasonable request.

We are grateful to all patients and patients' families from Ruijin Hospital, Shanghai Jiao Tong University School of Medicine.

Funding

This study was supported by the National Natural Science Foundation of China (82002773, 81772797, 81902320 and 81703532), Shanghai Municipal Education Commission–Gaofeng Clinical Medicine Grant Support (20172007), and Ruijin Hospital, Shanghai Jiao Tong University School of Medicine–"Guangci Excellent Youth Training Program" (GCQN-2017-A18).

Acknowledgements

Not applicable.

Author Contributions

ZW, YFL, XSC and KWS designed the study. ZW, FW, XYD and TEL performed the experiments. HYW, YHG and WJW analyzed the data. ZW and XYD wrote the manuscript. YFL, XSC and KWS revised the manuscript. All authors read and approved the final manuscript.

Competing Interests

The authors have declared that no competing interest exists.

References

1. Foulkes WD, Smith IE, Reis-Filho JS. Triple-negative breast cancer. N Engl J Med. 2010;363:1938–48.
2. Malorni L, Shetty PB, De Angelis C, Hilsenbeck S, Rimawi MF, Elledge R, et al. Clinical and biologic features of triple-negative breast cancers in a large cohort of patients with long-term follow-up. Breast cancer research treatment. 2012;136:795–804.
3. Qin S, Xu L, Yi M, Yu S, Wu K, Luo S. Novel immune checkpoint targets: moving beyond PD-1 and CTLA-4. Mol Cancer. 2019;18:155.

4. Schmid P, Adams S, Rugo HS, Schneeweiss A, Barrios CH, Iwata H, et al. Atezolizumab and Nab-Paclitaxel in Advanced Triple-Negative Breast Cancer. N Engl J Med. 2018;379:2108–21.
5. Vinayak S, Tolaney SM, Schwartzberg L, Mita M, McCann G, Tan AR, et al. Open-Label Clinical Trial of Niraparib Combined With Pembrolizumab for Treatment of Advanced or Metastatic Triple-Negative Breast Cancer. JAMA oncology. 2019;5:1132–40.
6. Adams S, Schmid P, Rugo HS, Winer EP, Loirat D, Awada A, et al. Pembrolizumab monotherapy for previously treated metastatic triple-negative breast cancer: cohort A of the phase II KEYNOTE-086 study. Annals of oncology: official journal of the European Society for Medical Oncology. 2019;30:397–404.
7. Bian L, Zhang H, Wang T, Zhang S, Song H, Xu M, et al. JS001, an anti-PD-1 mAb for advanced triple negative breast cancer patients after multi-line systemic therapy in a phase I trial. Annals of translational medicine. 2019;7:435.
8. Joyce JA, Fearon DT. T cell exclusion, immune privilege, and the tumor microenvironment. 348. New York: Science; 2015. pp. 74–80.
9. Hollmén M, Karaman S, Schwager S, Lisibach A, Christiansen AJ, Maksimow M, et al. G-CSF regulates macrophage phenotype and associates with poor overall survival in human triple-negative breast cancer. Oncoimmunology. 2016;5:e1115177.
10. Zhang WJ, Wang XH, Gao ST, Chen C, Xu XY, Sun Q, et al. Tumor-associated macrophages correlate with phenomenon of epithelial-mesenchymal transition and contribute to poor prognosis in triple-negative breast cancer patients. J Surg Res. 2018;222:93–101.
11. Noy R, Pollard JW. Tumor-associated macrophages: from mechanisms to therapy. Immunity. 2014;41:49–61.
12. Bartucci M, Dattilo R, Moriconi C, Pagliuca A, Mottolese M, Federici G, et al. TAZ is required for metastatic activity and chemoresistance of breast cancer stem cells. Oncogene. 2015;34:681–90.
13. Gao Y, Yang Y, Yuan F, Huang J, Xu W, Mao B, et al. TNFα-YAP/p65-HK2 axis mediates breast cancer cell migration. Oncogenesis. 2017;6:e383.
14. Sun S, Fei X, Mao Y, Wang X, Garfield DH, Huang O, et al. PD-1(+) immune cell infiltration inversely correlates with survival of operable breast cancer patients. Cancer immunology immunotherapy: CII. 2014;63:395–406.
15. Chen P, Zhao D, Li J, Liang X, Li J, Chang A, et al. Symbiotic Macrophage-Glioma Cell Interactions Reveal Synthetic Lethality in PTEN-Null Glioma. Cancer cell. 2019; 35: 868 – 84.e6.
16. Lei QY, Zhang H, Zhao B, Zha ZY, Bai F, Pei XH, et al. TAZ promotes cell proliferation and epithelial-mesenchymal transition and is inhibited by the hippo pathway. Mol Cell Biol. 2008;28:2426–36.
17. Wang Z, Li TE, Chen M, Pan JJ, Shen KW. miR-106b-5p contributes to the lung metastasis of breast cancer via targeting CNN1 and regulating Rho/ROCK1 pathway. Aging. 2020;12:1867–87.
18. Czepielewski RS, Porto BN, Rizzo LB, Roesler R, Abujamra AL, Pinto LG, et al. Gastrin-releasing peptide receptor (GRPR) mediates chemotaxis in neutrophils. Proc Natl Acad Sci USA. 2012;109:547–52.

19. Goodarzi K, Goodarzi M, Tager AM, Luster AD, von Andrian UH. Leukotriene B4 and BLT1 control cytotoxic effector T cell recruitment to inflamed tissues. Nature immunology. 2003;4:965–73.
20. Su S, Liu Q, Chen J, Chen J, Chen F, He C, et al. A positive feedback loop between mesenchymal-like cancer cells and macrophages is essential to breast cancer metastasis. Cancer cell. 2014;25:605–20.
21. Miao YR, Zhang Q, Lei Q, Luo M, Xie GY, Wang H, et al. ImmuCellAI: A Unique Method for Comprehensive T-Cell Subsets Abundance Prediction and its Application in Cancer Immunotherapy. Adv Sci (Weinh). 2020;7:1902880.
22. Sonja H¨anzelmann RC. Justin Guinney. GSVA: gene set variation analysis for.
23. microarray and RNA-Seq data. BMC Bioinform. 2013;14:7.
24. Cerami E, Gao J, Dogrusoz U, Gross BE, Sumer SO, Aksoy BA, et al. The cBio cancer genomics portal: an open platform for exploring multidimensional cancer genomics data. Cancer Discov. 2012;2:401–4.
25. Győrffy B, Lanczky A, Eklund AC, Denkert C, Budczies J, Li Q, et al. An online survival analysis tool to rapidly assess the effect of 22,277 genes on breast cancer prognosis using microarray data of 1,809 patients. Breast cancer research treatment. 2010;123:725–31.
26. Yu M, Peng Z, Qin M, Liu Y, Wang J, Zhang C, et al. Interferon-gamma induces tumor resistance to anti-PD-1 immunotherapy by promoting YAP phase separation. Mol Cell. 2021;81:1216-30 e9.
27. Lin H, Lee E, Hestir K, Leo C, Huang M, Bosch E, et al. Discovery of a cytokine and its receptor by functional screening of the extracellular proteome. 320. New York: Science; 2008. pp. 807–11.
28. DeNardo DG, Ruffell B. Macrophages as regulators of tumour immunity and immunotherapy. Nature reviews Immunology. 2019;19:369–82.
29. Yu G, Bing Y, Zhu S, Li W, Xia L, Li Y, et al. Activation of the interleukin-34 inflammatory pathway in response to influenza A virus infection. Am J Med Sci. 2015;349:145–50.
30. Zwicker S, Martinez GL, Bosma M, Gerling M, Clark R, Majster M, et al. Interleukin 34: a new modulator of human and experimental inflammatory bowel disease. Clinical science (London, England: 1979). 2015; 129: 281 – 90.
31. Baghdadi M, Wada H, Nakanishi S, Abe H, Han N, Putra WE, et al. Chemotherapy-Induced IL34 Enhances Immunosuppression by Tumor-Associated Macrophages and Mediates Survival of Chemoresistant Lung Cancer Cells. Cancer research. 2016;76:6030–42.
32. Endo H, Hama N, Baghdadi M, Ishikawa K, Otsuka R, Wada H, et al. Interleukin-34 expression in ovarian cancer: a possible correlation with disease progression. Int Immunol. 2020;32:175–86.
33. Joyce JA, Pollard JW. Microenvironmental regulation of metastasis. Nat Rev Cancer. 2009;9:239–52.
34. Wagner J, Rapsomaniki MA, Chevrier S, Anzeneder T, Langwieder C, Dykgers A, et al. A Single-Cell Atlas of the Tumor and Immune Ecosystem of Human Breast Cancer. Cell. 2019;177:1330–45.e18.
35. Qian BZ, Pollard JW. Macrophage diversity enhances tumor progression and metastasis. Cell. 2010;141:39–51.

36. Cassetta L, Fragkogianni S, Sims AH, Swierczak A, Forrester LM, Zhang H, et al. Human Tumor-Associated Macrophage and Monocyte Transcriptional Landscapes Reveal Cancer-Specific Reprogramming, Biomarkers, and Therapeutic Targets. Cancer cell. 2019;35:588–602.e10.
37. Flavell RA, Sanjabi S, Wrzesinski SH, Licona-Limón P. The polarization of immune cells in the tumour environment by TGFbeta. Nature reviews Immunology. 2010;10:554–67.
38. Wang Y, Tu K, Liu D, Guo L, Chen Y, Li Q, et al. p300 Acetyltransferase Is a Cytoplasm-to-Nucleus Shuttle for SMAD2/3 and TAZ Nuclear Transport in Transforming Growth Factor β-Stimulated Hepatic Stellate Cells. Hepatology (Baltimore, Md). 2019; 70: 1409–23.
39. Miranda MZ, Bialik JF, Speight P, Dan Q, Yeung T, Szászi K, et al. TGF-β1 regulates the expression and transcriptional activity of TAZ protein via a Smad3-independent, myocardin-related transcription factor-mediated mechanism. J Biol Chem. 2017;292:14902–20.
40. Janse van Rensburg HJ, Azad T, Ling M, Hao Y, Snetsinger B, Khanal P, et al. The Hippo Pathway Component TAZ Promotes Immune Evasion in Human Cancer through PD-L1. Cancer research. 2018;78:1457–70.
41. Sanmamed MF, Chen L. A Paradigm Shift in Cancer Immunotherapy: From Enhancement to Normalization. Cell. 2018;175:313–26.
42. Chen L, Han X. Anti-PD-1/PD-L1 therapy of human cancer: past, present, and future. J Clin Investig. 2015;125:3384–91.
43. Pitt JM, Vétizou M, Daillère R, Roberti MP, Yamazaki T, Routy B, et al. Resistance Mechanisms to Immune-Checkpoint Blockade in Cancer: Tumor-Intrinsic and -Extrinsic Factors. Immunity. 2016;44:1255–69.
44. Pyonteck SM, Akkari L, Schuhmacher AJ, Bowman RL, Sevenich L, Quail DF, et al. CSF-1R inhibition alters macrophage polarization and blocks glioma progression. Nat Med. 2013;19:1264–72.
45. Neubert NJ, Schmittnaegel M, Bordry N, Nassiri S, Wald N, Martignier C, et al. T cell-induced CSF1 promotes melanoma resistance to PD1 blockade. Science translational medicine. 2018; 10.
46. Tap WD, Gelderblom H, Palmerini E, Desai J, Bauer S, Blay JY, et al. Pexidartinib versus placebo for advanced tenosynovial giant cell tumour (ENLIVEN): a randomised phase 3 trial. Lancet. 2019;394:478–87.

Figures

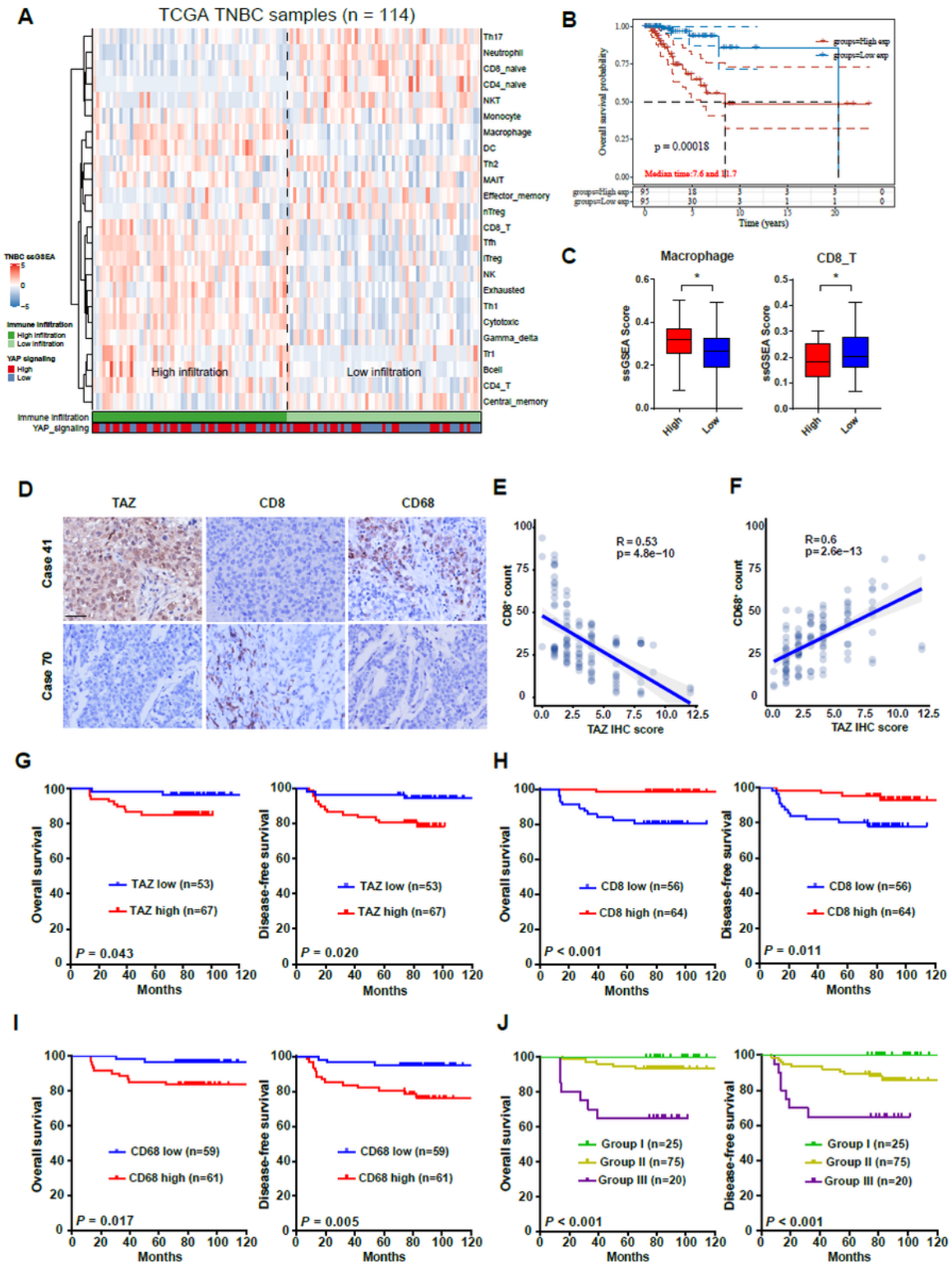

Figure 1

The relationship between Hippo pathway and immune cell infiltration and its clinical significance in TNBC patients. (A) The landscape of immune cell infiltration of TNBC patients in the TCGA training cohort. High or low infiltration based on immune infiltration score estimated by ImmuCellAI. The activity of conserved YAP signature was estimated by GSVA algorithm. (B) Correlation of combined activity of conserved YAP signature with overall survival in TCGA TNBC patients. (C) Macrophage and CD8+ T cells infiltration

between high and low activity of conserved YAP signature. (D) Representative images of IHC staining of TAZ, CD8, and CD68 in TNBC samples (up: high expression of TAZ and CD68 and low expression of CD8; bottom: low expression of TAZ and CD68 and high expression of CD8). Scale bar, 50μm. (E) Scatterplot of intratumoral CD8+ T cell counts according to TAZ IHC scores in TNBC samples. (F) Scatterplot of intratumoral CD68+ TAM counts according to TAZ IHC scores in TNBC samples. (G) Prognostic values of TAZ expression for OS and DFS. (H) Prognostic values of intratumoral CD8+ T cell counts for OS and DFS. (I) Prognostic values of intratumoral CD68+ TAM counts for OS and DFS. (J) Prognostic values of the combination of TAZ expression, CD8+ T cells, and CD68+ TAMs for OS and DFS (Group I: patients with low TAZ expression, an increased number of T cells, and fewer TAMs; Group III: patients with high TAZ expression, fewer T cells, and an increased number of TAMs; Group II: the remaining patients). Student's t-test in(C), Pearson's correlation test in (E) and (F), and Kaplan-Meier analysis in (B, G-J). DFS: disease-free survival; IHC: immunohistochemistry; OS: overall survival; TAM: tumor-associated macrophage; TAZ: transcriptional coactivator with PDZ-binding motif; TNBC: triple-negative breast cancer.

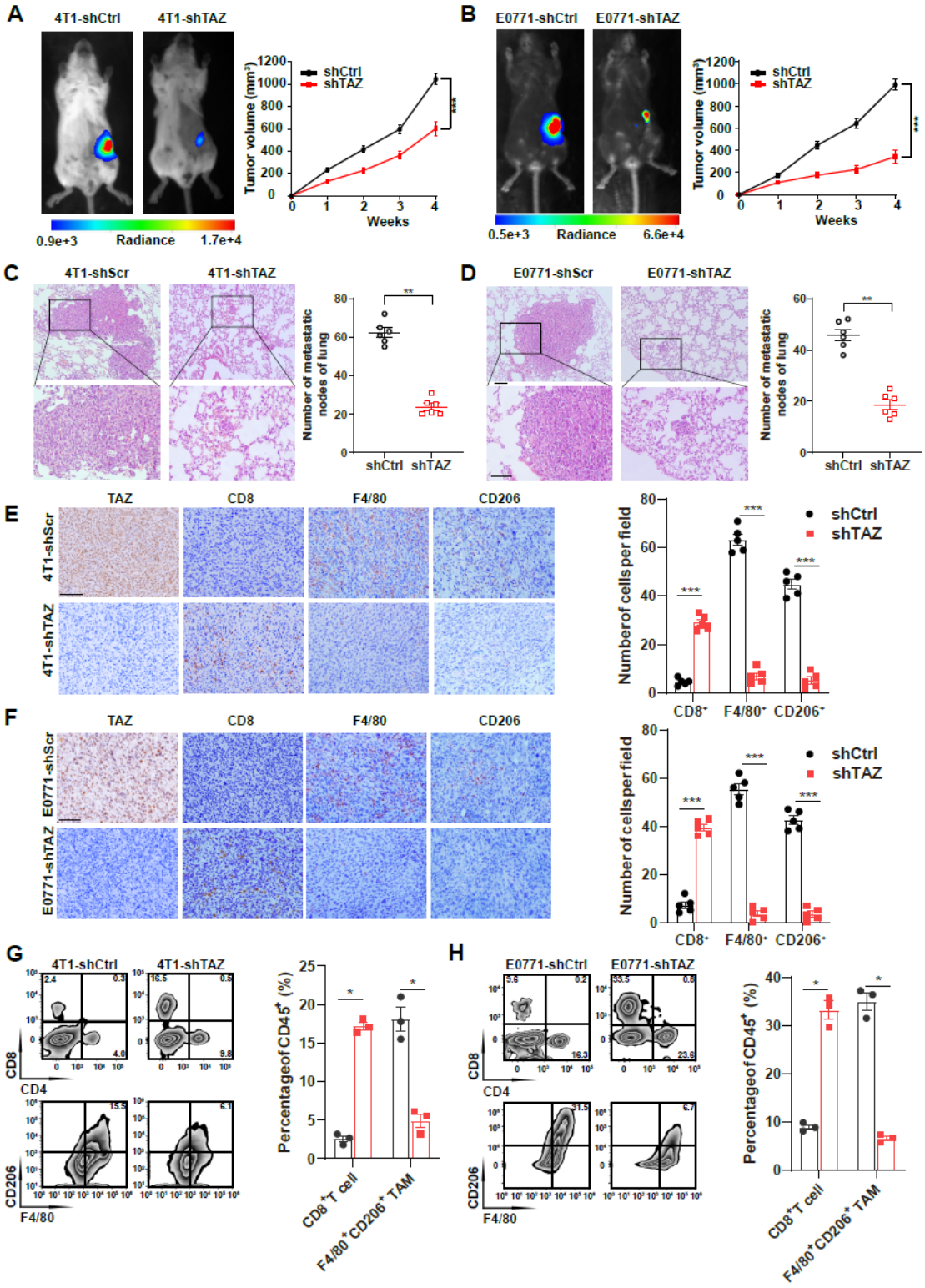

Figure 2

Role of TAZ in the immunosuppressive microenvironment and progression of TNBC. (A, B) 4T1 cells (A) and E0771 cells (B) with TAZ silencing vector lentivirus (shTAZ) or control vector lentivirus (shCtrl) were orthotopically inoculated into mice (n = 6 mice/group). Representative bioluminescence images of xenograft tumors are shown at day 28 after injection of 4T1 or E0771 cells (left) and tumor growth in each group (right). 4T1-shTAZ, E0771-shTAZ, and their -shCtrl stable cells were injected into the tail veins

of mice (n = 6 mice/group). (C, D) Representative images of H&E staining of lung tissues (left) and the number of lung metastatic nodules (right) in 4T1-shTAZ-derived (C) and E0771-shTAZ-derived (D) models. Scale bars, 100μm. (E, F) Representative images and quantification of IHC staining of TAZ, CD8, F4/80, and CD206 in 4T1-derived (E) and E0771-derived (F) xenograft tumors. Scale bars, 100μm. (G, H) Representative images and quantification of flow cytometry analysis of tumor-infiltrating CD8+ T cells and F4/80+ CD206+ TAMs in 4T1-derived (G) and E0771-derived (H) xenograft tumors. * $P < 0.05$, ** $P < 0.01$ and *** $P < 0.001$, Student's t-test in (A-D), and two-way ANOVA in (E-H). ANOVA: analysis of variance; H&E: hematoxylin-eosin; TAM: tumor-associated macrophage; TAZ: transcriptional coactivator with PDZ-binding motif; TNBC: triple-negative breast cancer.

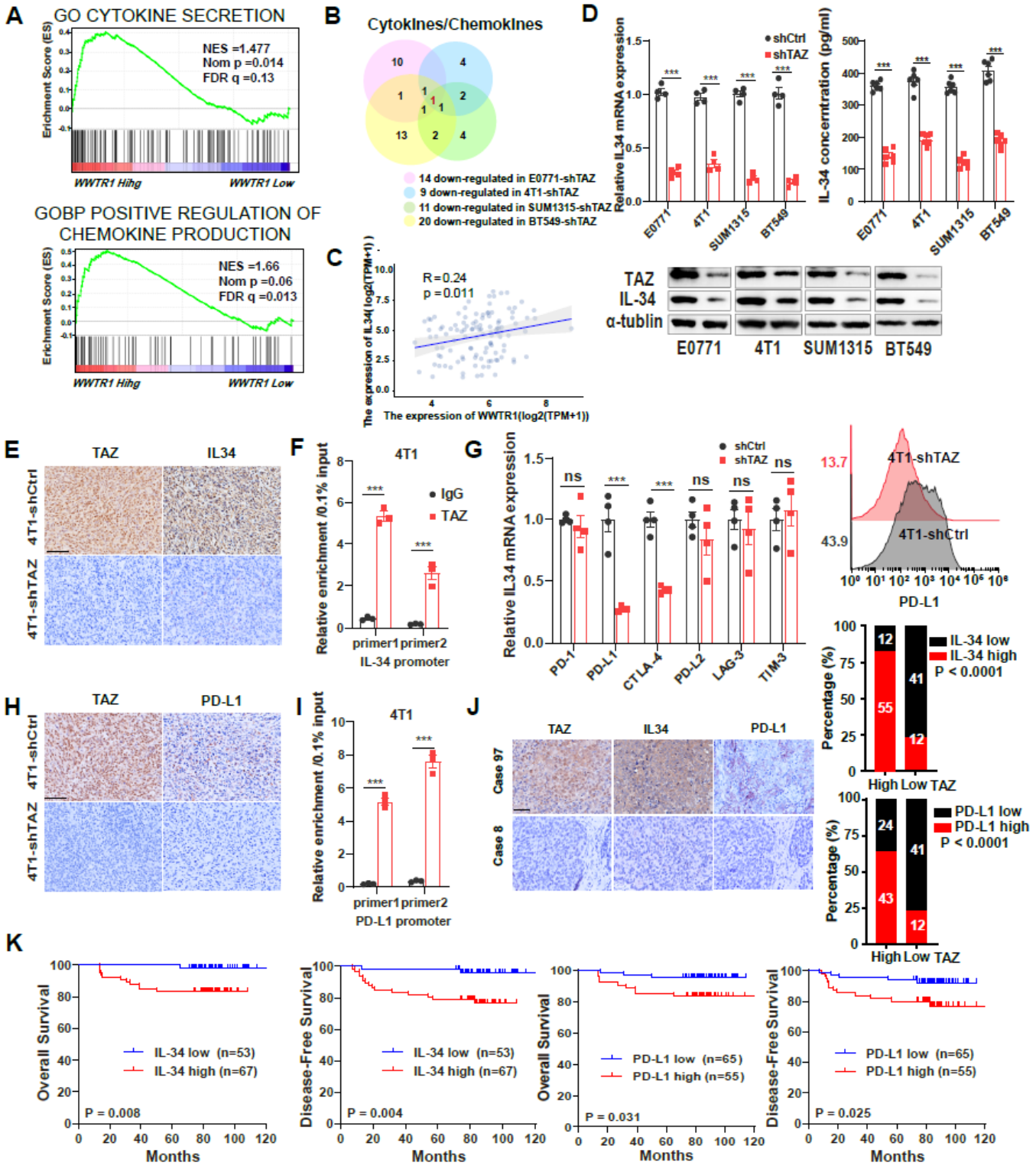

Figure 3

Effect of TAZ expression on the immune and inflammatory profile, and IL-34 and PD-L1 expression. (A) Representative cytokines and chemokines production gene sets enriched in GSEA of TCGA TNBC patients with low or high expression of TAZ. (B) Venn diagrams showing IL-34 as the downstream target of TAZ according to four groups of downregulated cytokines/chemokines: (1) in E0771-shTAZ xenograft tumors, (2) in 4T1-shTAZ xenograft tumors, (3) in SUM1315-shTAZ cells, and (4) in BT549-shTAZ cells. (C)

Pearson correlation analysis between TAZ gene expression and IL-34 mRNA expression in the TCGA cohort. (D) RT-qPCR and western blot analysis of IL-34 expression (left) and ELISA analysis of IL-34 levels (right) in E0771, 4T1, SUM1315, and BT549 cells. (E) Representative images of IHC staining of TAZ and IL-34 in 4T1-derived xenograft tumors. Scale bars, 100μm. (F) Chromatin immunoprecipitation-qPCR of TAZ on the IL-34 promoter. (G) RT-qPCR analysis (left) and flow cytometry analysis (right) of PD-L1 expression in 4T1 xenograft tumors. (H) Representative images of IHC staining of PD-L1 expression in 4T1 xenograft tumors. Scale bars, 100μm. (I) Chromatin immunoprecipitation-qPCR of TAZ on the PD-L1 promoter. (J) Representative images of IHC staining of TAZ, IL-34, and PD-L1 in TNBC samples (left up: high expression of TAZ, IL-34, and PD-L1; left bottom: low expression of TAZ, IL-34, and PD-L1) and their expression correlations (right). Scale bar, 50μm. (K) Prognostic values of IL-34 and PD-L1 expression for overall survival and disease-free survival in TNBC patients. *** $P < 0.001$, Pearson's correlation test in (C), two-way ANOVA in (D) and (F-G, I), Chi-square test in (J), and Kaplan-Meier analysis in (K). ANOVA: analysis of variance; CTLA-4: cytotoxic T-lymphocyte associated protein 4; ELISA: enzyme linked immunosorbent assay; IHC: immunohistochemistry; IL-34: interleukin 34; PD-1: programmed death 1; PD-L1: programmed death ligand 1; PD-L2: programmed death ligand 2; RT-qPCR: real-time quantitative polymerase chain reaction; TAZ: transcriptional coactivator with PDZ-binding motif; TCGA: The Cancer Genome Atlas; TNBC: triple-negative breast cancer; TIM-3: T-cell immunoglobulin and mucin domain-containing protein 3.

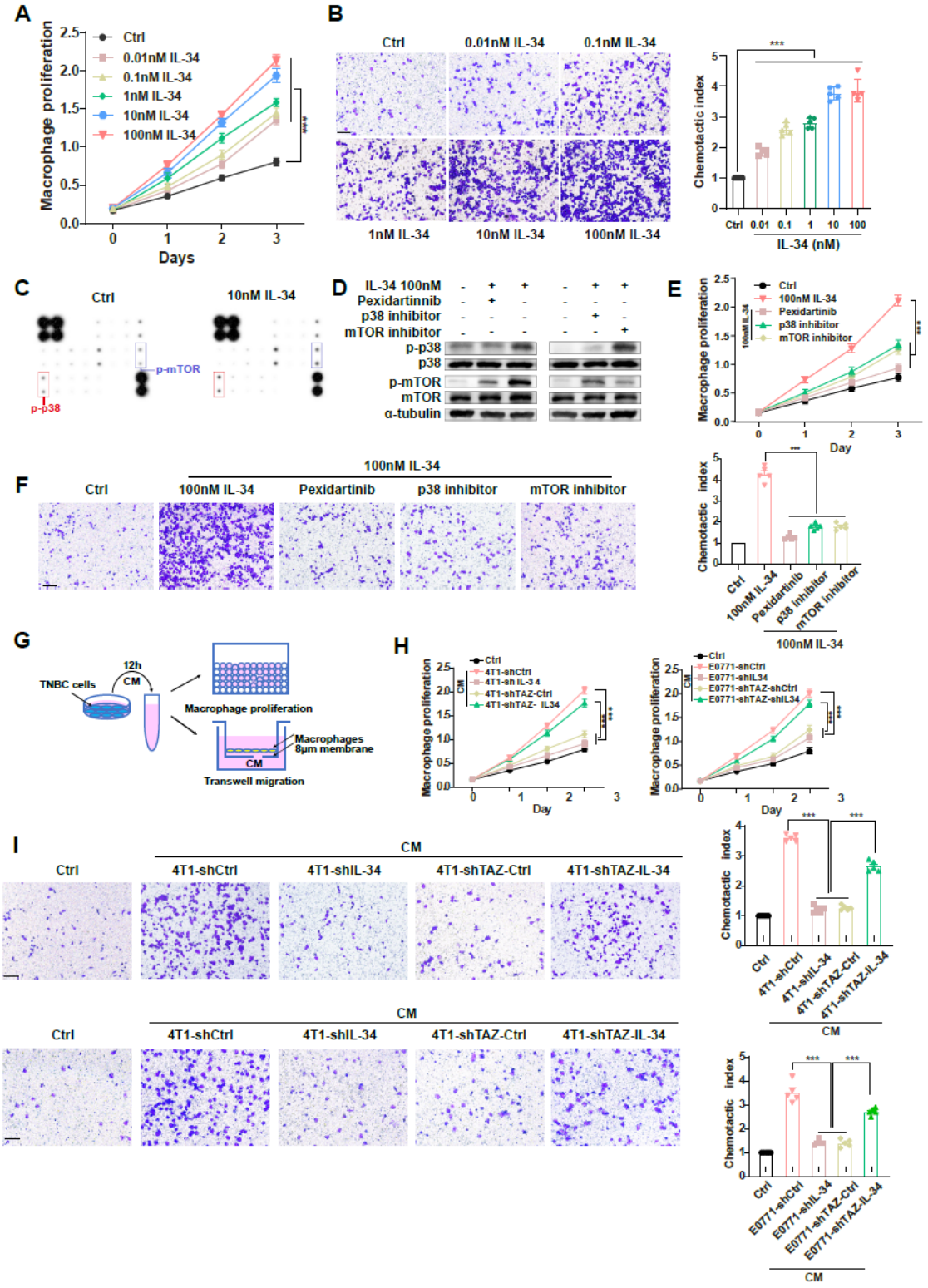

Figure 4

The TAZ/IL-34 axis activated p38 and mTOR signaling and promoted macrophage proliferation and migration. (A, B) IL-34-induced concentration-dependent proliferation (A) and chemotactic migration (B) of macrophages within the range of 0.01-100nM. Scale bar, 100μm. (C) Phospho-kinase array analysis of downstream signaling pathways activated by IL-34 treatment. (D) Western blot analysis of p38 and mTOR phosphorylation levels in macrophages after exposure to IL-34 and treatment with a CSF-1R

inhibitor, p38 inhibitor, or mTOR inhibitor, compared to the IL-34 treatment group. (E, F) Proliferation (E) and chemotactic migration (F) of macrophages were assessed after exposure to IL-34 and treatment with a CSF-1R inhibitor, p38 inhibitor, or mTOR inhibitor, compared to the IL-34 treatment group. Scale bar, 100μm. (G) A schematic diagram showing macrophages being cultured with CM derived from TNBC cells. (H, I) Proliferation (H) and chemotactic migration (I) of macrophages were measured after stimulation with different CMs and compared with those of other groups. Scale bars, 100μm. *** $P < 0.001$, two-way ANOVA in (A), (E) and (H), and one-way ANOVA in (B), (F) and (I). ANOVA: analysis of variance; CM: conditioned medium; CSF-1R: colony-stimulating factor 1 receptor; IL-34: interleukin 34; TAZ: transcriptional coactivator with PDZ-binding motif; TNBC: triple-negative breast cancer.

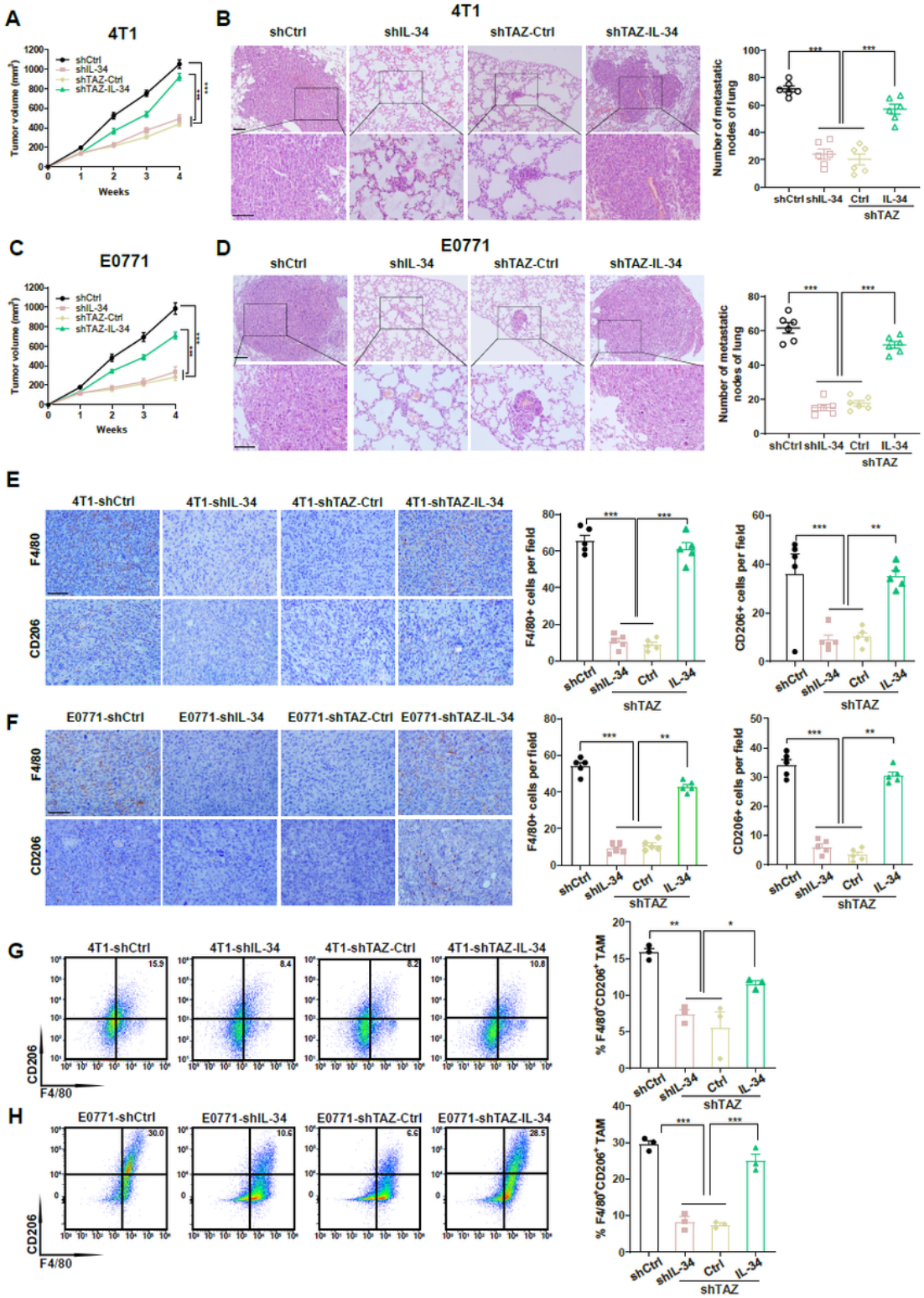

Figure 5

Effect of the TAZ/IL-34 axis on TAM infiltration and TNBC progression. (A, C) 4T1 cells (A) and E0771 cells (C) with control lentivirus vector (shCtrl), IL-34 silencing lentivirus vector (shIL-34), TAZ silencing lentivirus vector (shTAZ-Ctrl), or TAZ silencing and IL-34 overexpression lentivirus vectors (shTAZ-IL-34) were orthotopically inoculated into mice (n = 6 mice/group). Tumor growth from each group is shown. (B, D) 4T1 (B) and E0771 (D) -shCtrl, -shIL-34, -shTAZ-Ctrl, and -shTAZ-IL-34 stable cells were injected into the

tail veins of mice (n = 6 mice/group). Representative images of H&E staining of lung tissues and the number of lung metastatic nodules are shown. Scale bars, 100μm. (E, F) Representative images and quantification of IHC staining of F4/80 and CD206 in 4T1-derived (E) and E0771-derived (F) xenograft tumors. Scale bars, 100μm. (G, H) Representative images and quantification of flow cytometry analysis of tumor-infiltrating F4/80+ CD206+ TAMs in 4T1-derived (G) and E0771-derived (H) xenograft tumors. * $P < 0.05$, ** $P < 0.01$ and *** $P < 0.001$, two-way ANOVA in (A) and (C), and one-way ANOVA in (B), (D) and (E-H). ANOVA: analysis of variance; H&E: hematoxylin-eosin; IHC: immunohistochemistry; IL-34: interleukin 34; TAM: tumor-associated macrophage; TAZ: transcriptional coactivator with PDZ-binding motif; TNBC: triple-negative breast cancer.

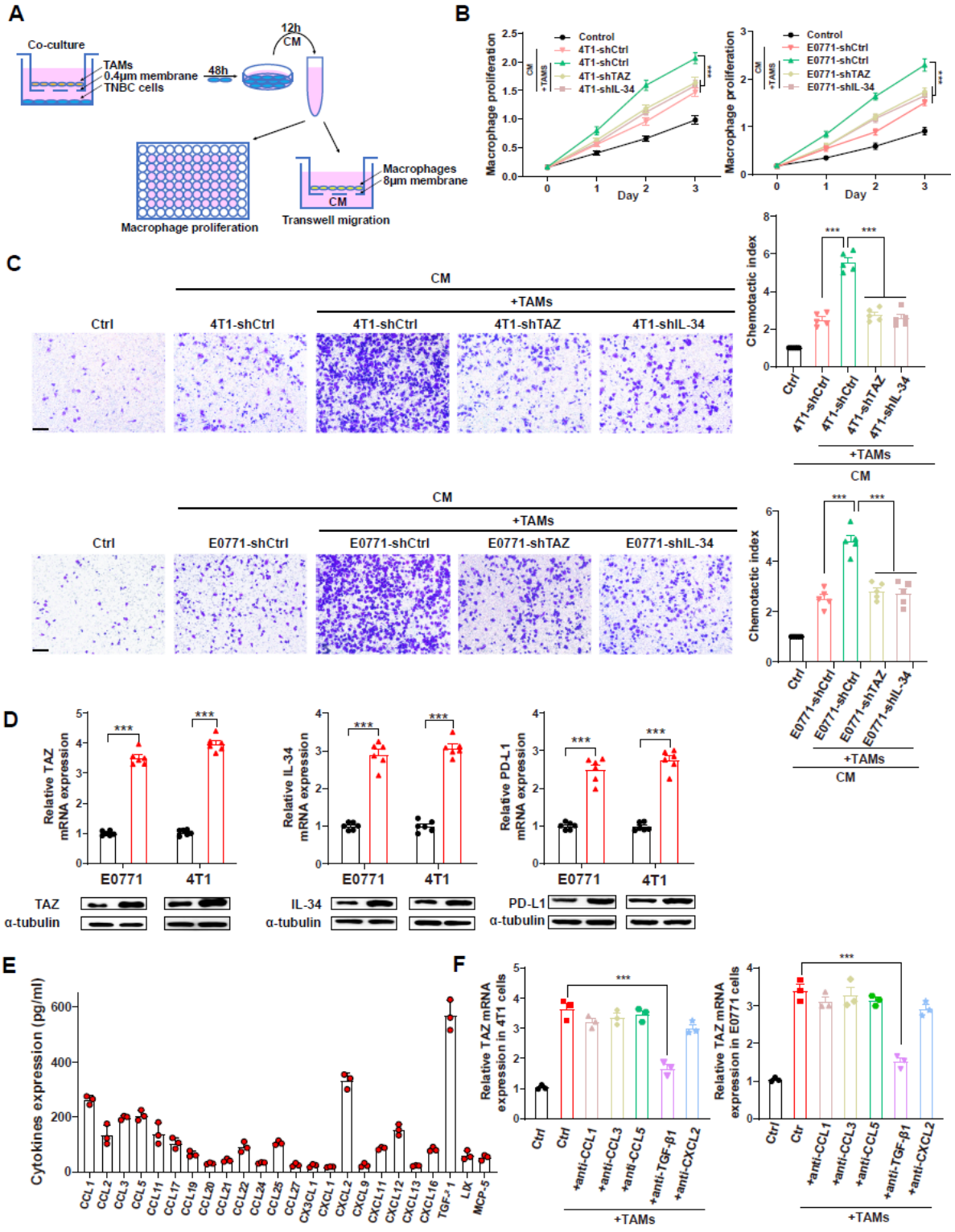

Figure 6

TAM-derived TGF-β1 promoted TAZ expression in TNBC cells. (A) A schematic diagram showing that TNBC cells were co-cultured with TAMs in a Transwell system for 48 h and then were re-plated and cultured after 12 h. The CM was obtained for further experiments. (B, C) Proliferation (B) and chemotactic migration (C) of macrophages were assessed following exposure to 4T1 and E0771 cells after co-culture with TAMs. Scale bars, 100μm. (D) RT-qPCR analysis of TAZ, IL-34, and PD-L1 expression in 4T1 and

E0771 cells after co-culture with TAMs. (E) Cytokine array analysis of supernatants from TAMs. (F) RT-qPCR and western blot analysis of TAZ expression in 4T1 and E0771 cells after co-culture with TAMs and treatment with neutralizing antibodies, compared with the control group. *** P < 0.001, two-way ANOVA in (B) and (D), and one-way ANOVA in (C) and (F). ANOVA: analysis of variance; IL-34: interleukin 34; PD-L1: programmed death ligand 1; RT-qPCR: real-time quantitative polymerase chain reaction; TAM: tumor-associated macrophage; TAZ: transcriptional coactivator with PDZ-binding motif; TGF-β1: transforming growth factor beta 1; TNBC: triple-negative breast cancer.

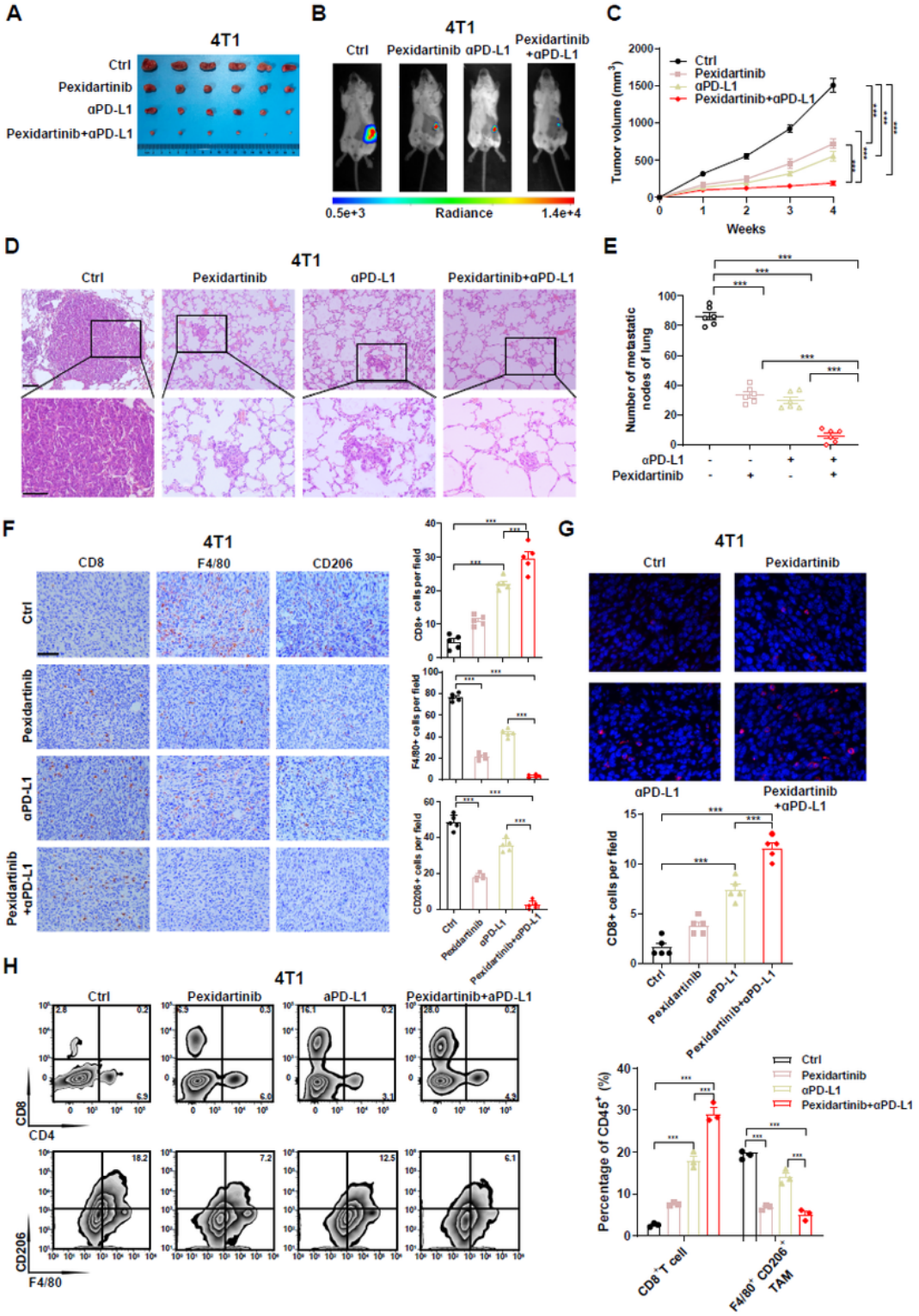

Figure 7

CSF-1R blockade sensitized TNBC to anti-PD-L1-mediated immunotherapy by reversing the immunosuppressive tumor microenvironment. 4T1 cells were orthotopically inoculated into mice (n = 6 mice/group). When tumors reached 50 mm3, mice were randomly assigned to the isotype control, pexidartinib (40 mg/kg orally once a day), anti-PD-L1 (200μg injected intraperitoneally every 3 days), or pexidartinib plus anti-PD-L1 group. (A) Representative image of the tumors from each group after the mice were sacrificed. (B, C) Representative bioluminescence images of xenograft tumors at day 28 after injection of 4T1 cells (B) and tumor growth in each group (C). 4T1 cells were injected into the tail veins of mice (n = 6 mice/group). Mice were randomly assigned to four treatment groups. (D, E) Representative images of H&E staining of lung tissues (D) and the number of lung metastatic nodules (E). Scale bars, 100μm. (F) Representative images and quantification of IHC staining of CD8, F4/80, and CD206 in xenograft tumors from each treatment group. Scale bars, 100μm. (G) Representative images and quantification of immunofluorescence confocal microscopy of CD8+ T cells in xenograft tumors. (H) Representative images and quantification of flow cytometry analysis of tumor-infiltrating CD8+ T cells and F4/80+ CD206+ TAMs in xenograft tumors from each treatment group. *** $P < 0.001$, two-way ANOVA in (C) and (H), and one-way ANOVA in (E-G). ANOVA: analysis of variance; CSF-1R: colony-stimulating factor 1 receptor; H&E: hematoxylin-eosin; IHC: immunohistochemistry; PD-L1: programmed death ligand 1; TAM: tumor-associated macrophage.

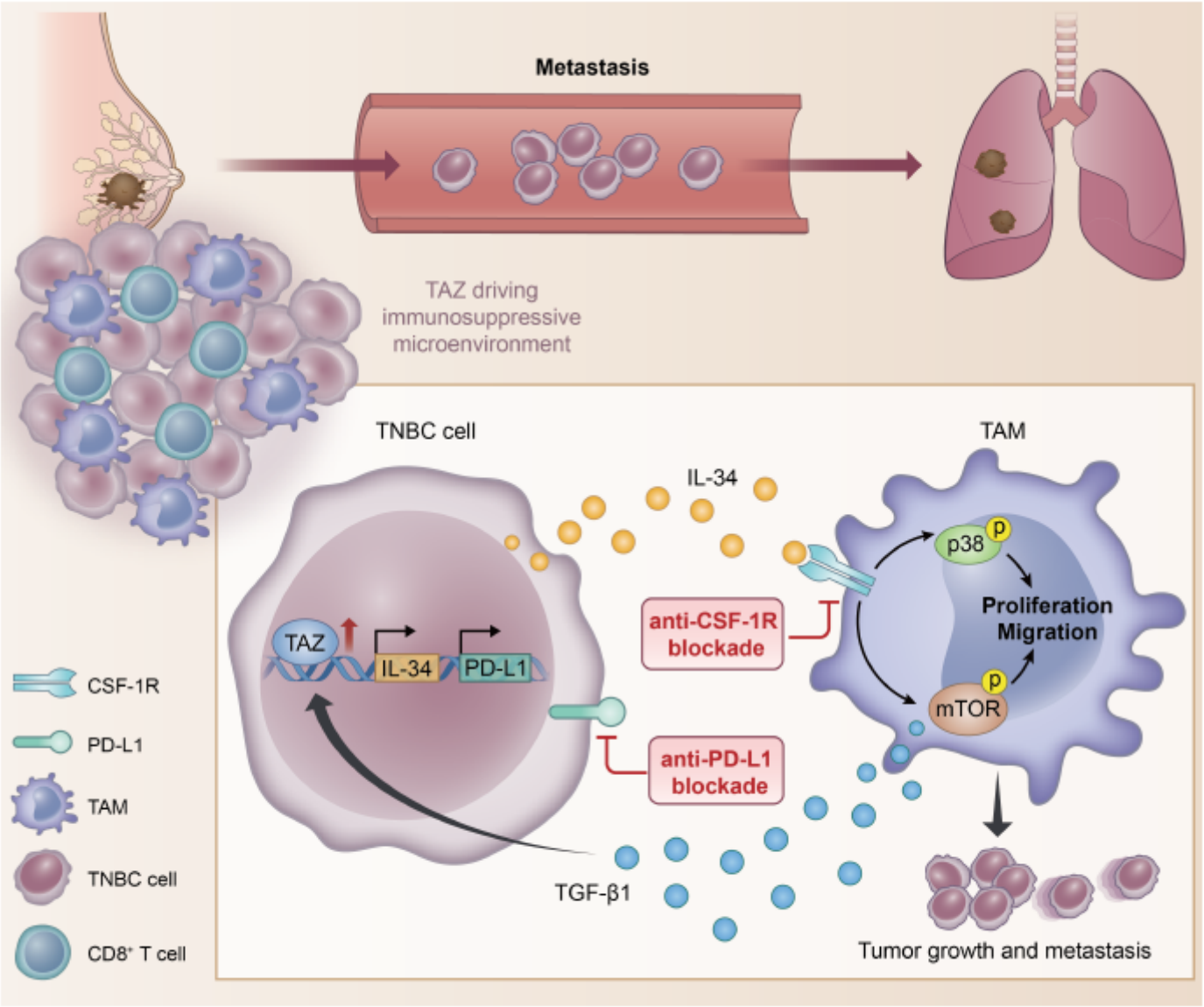

Figure 8

Proposed working model. TAZ drives the immunosuppressive phenotype in TNBC by decreasing intratumoral T cell infiltration and promoting TAM recruitment. As a signaling hub in the tumor microenvironment, TAZ shifts the immune and inflammatory profile and directly regulates IL-34 and PD-L1 expression. IL-34 promotes the proliferation and migration of TAMs by activating the p38 and mTOR signaling pathways. TAM-derived TGF-β1 promotes TAZ expression in TNBC cells, thus forming a positive feedback loop between TNBC cells and TAMs. Blocking the TAZ/IL-34/CSF-1R axis reduces TAM infiltration, activates intratumoral CD8+ T cells, and sensitizes TNBC to anti-PD-L1-mediated immunotherapy. CSF-1R: colony-stimulating factor 1 receptor; IL-34: interleukin 34; PD-L1: programmed death ligand 1; TAM: tumor-associated macrophage; TAZ: transcriptional coactivator with PDZ-binding motif; TGF-β1: transforming growth factor beta 1; TNBC: triple-negative breast cancer.

Supplementary Files

This is a list of supplementary files associated with this preprint. Click to download.

- FigureS1.pdf
- FigureS2.pdf
- FigureS3.pdf
- FigureS4.pdf
- FigureS5.pdf
- FigureS6.pdf
- FigureS7.pdf
- FigureS8.pdf
- FigureS9.pdf
- FigureS10.pdf
- SupplementaryMaterials.docx